

Rps14 haploinsufficiency causes a block in erythroid differentiation mediated by S100A8 and S100A9

Rebekka K Schneider^{1,2}, Monica Schenone³, Monica Ventura Ferreira², Rafael Kramann⁴, Cailin E Joyce⁵, Christina Hartigan³, Fabian Beier², Tim H Brümmendorf², Ulrich Germing⁶, Uwe Platzbecker⁷, Guntram Büsche⁸, Ruth Knüchel⁹, Michelle C Chen¹, Christopher S Waters¹, Edwin Chen¹, Lisa P Chu¹, Carl D Novina⁵, R Coleman Lindsley^{1,5}, Steven A Carr² & Benjamin L Ebert^{1,3}

Impaired erythropoiesis in the deletion 5q (del(5q)) subtype of myelodysplastic syndrome (MDS) has been linked to heterozygous deletion of *RPS14*, which encodes the ribosomal protein small subunit 14. We generated mice with conditional inactivation of *Rps14* and demonstrated an erythroid differentiation defect that is dependent on the tumor suppressor protein p53 (encoded by *Trp53* in mice) and is characterized by apoptosis at the transition from polychromatic to orthochromatic erythroblasts. This defect resulted in age-dependent progressive anemia, megakaryocyte dysplasia and loss of hematopoietic stem cell (HSC) quiescence. As assessed by quantitative proteomics, mutant erythroblasts expressed higher levels of proteins involved in innate immune signaling, notably the heterodimeric S100 calcium-binding proteins S100a8 and S100a9. S100a8—whose expression was increased in mutant erythroblasts, monocytes and macrophages—is functionally involved in the erythroid defect caused by the *Rps14* deletion, as addition of recombinant S100a8 was sufficient to induce a differentiation defect in wild-type erythroid cells, and genetic inactivation of *S100a8* expression rescued the erythroid differentiation defect of *Rps14*-haploinsufficient HSCs. Our data link *Rps14* haploinsufficiency in del(5q) MDS to activation of the innate immune system and induction of S100A8-S100A9 expression, leading to a p53-dependent erythroid differentiation defect.

Isolated, interstitial deletion of chromosome 5q in patients with MDS is associated with a clinical phenotype, termed the 5q- syndrome, that is characterized by a severe macrocytic anemia, a normal or elevated platelet count with hypolobated micromegakaryocytes and a low rate of progression to acute myelogenous leukemia^{1–3}. The severe macrocytic anemia in del(5q) MDS patients has been linked to haploinsufficiency of RPS14 (ref. 4). In a screen for genes in the chromosome 5q33 common-deleted region associated with the 5q- syndrome, only small hairpin RNAs (shRNAs) targeting the *RPS14* gene caused a severe block in erythroid differentiation, whereas forced overexpression of *RPS14* in cells from MDS patients with the 5q deletion rescued erythropoiesis⁴.

Germline, heterozygous inactivating mutations or deletions of *RPS19* and other ribosomal protein genes cause Diamond-Blackfan anemia (DBA), a disorder that, like del(5q) MDS, is characterized by macrocytic anemia^{5–9}. Ribosomal dysfunction is sensed by the p53 pathway, leading to apoptosis and cell cycle arrest. Decreased expression of individual ribosomal proteins, including that of RPS19 and RPS14, increases p53 protein levels and p53 target-gene expression in cell lines, primary human hematopoietic progenitor cells and patient

samples^{10–12}. Pharmacologic or genetic inactivation of p53 rescues the differentiation defect in cells with ribosomal haploinsufficiency in multiple model systems^{7,8,10,13}.

Several *in vivo* models of ribosome dysfunction have been described¹⁴. A mouse model with a hematopoietic-specific, heterozygous deletion of *Rps6* recapitulates the erythroid phenotype of del(5q) MDS and DBA, and this phenotype is rescued by p53 inactivation^{7,8,15}; however, *RPS6* inactivation has not been described in either DBA or MDS. To model del(5q) MDS in mice, a series of DNA segments syntenic to the commonly deleted region on human chromosome 5, including those containing *Rps14*, was conditionally deleted from the HSC compartment¹³. Heterozygous loss of this region resulted in a macrocytic anemia and dysplastic megakaryocytes, recapitulating aspects of the 5q- syndrome. The smallest deletion tested that resulted in the erythroid defect included *Rps14* and seven other genes.

To investigate the hematologic phenotype and molecular consequences specific to *Rps14* haploinsufficiency *in vivo* and to explore the role of this gene in del(5q) MDS, we generated a mouse model with conditional *Rps14* inactivation.

¹Division of Hematology, Department of Medicine, Brigham and Women's Hospital, Harvard Medical School, Boston, Massachusetts, USA. ²Department of Hematology, Hemostaseology, Oncology and Stem Cell Transplantation, University Hospital Rheinisch-Westfälische Technische Hochschule (RWTH) Aachen, Aachen, Germany. ³Broad Institute of Harvard University and the Massachusetts Institute of Technology, Cambridge, Massachusetts, USA. ⁴Renal Division, Brigham and Women's Hospital, Boston, Massachusetts, USA. ⁵Dana-Farber Cancer Institute, Boston, Massachusetts, USA. ⁶Department of Hematology, Oncology and Clinical Immunology, Heinrich Heine University, Düsseldorf, Germany. ⁷Department of Medicine I, University Hospital Carl Gustav Carus, University of Technology, Dresden, Germany. ⁸Institute of Pathology, Hannover Medical School, Hannover, Germany. ⁹Institute of Pathology, University Hospital Rheinisch-Westfälische Technische Hochschule (RWTH) Aachen, Aachen, Germany. Correspondence should be addressed to B.L.E. (bebert@partners.org).

Received 11 October 2015; accepted 14 January 2016; published online 15 February 2016; doi:10.1038/nm.4047

RESULTS

***Rps14* haploinsufficiency induces a p53-dependent erythroid differentiation defect in late-stage erythroblasts**

We generated a conditional *Rps14*-knockout model in which exons 2–4 are flanked by *loxP* sites (floxed *Rps14*, or *Rps14^{fl/fl}*, mice) (Supplementary Fig. 1a). After crossing these mice to *Mx1-Cre⁺* transgenic mice, in which the Cre recombinase is under the control of the hematopoietic cell-specific *Mx1* promoter, we induced *Rps14* excision in hematopoietic cells by treatment of 6- to 8-week-old mice with polyinosinic-polycytidylic acid (poly(I:C)) and confirmed haploinsufficient expression (approximately 50% of normal levels) of *Rps14* (Supplementary Fig. 1b,c). Mice with heterozygous deletion of *Rps14* in hematopoietic cells (hereafter referred to as *Rps14*-haploinsufficient mice) developed a progressive anemia (Fig. 1a and Supplementary Fig. 1d,e). At approximately 550 d of age, the reticulocyte count of *Rps14*-haploinsufficient mice decreased precipitously and was associated with death in a subset of these mice (Fig. 1a,b).

We next determined whether *Rps14* haploinsufficiency causes a discrete, stage-specific defect in erythroid development. We characterized the stages of erythropoiesis by flow cytometry on the basis of the expression of Ter119 (also called lymphocyte antigen 76; Ly76) and CD71 (also known as transferrin receptor protein 1; TfR1) (which we refer to as RI, RII, RIII and RIV; Supplementary Fig. 1d). At 18 months of age, *Rps14*-haploinsufficient mice had impaired erythropoiesis at the transition from CD71⁺Ter119⁺ basophilic and early chromatophilic erythroblasts (the RII stage) to CD71^{intermediate}Ter119⁺ polychromatophilic

(RIII) to CD71^{low}Ter119⁺ orthochromatophilic erythroblasts and enucleated erythrocytes (RIV) (Fig. 1c). Moreover, *Rps14*-haploinsufficient mice had significant splenomegaly due to expansion of the early-erythroid compartment (Fig. 1d and Supplementary Fig. 1i). Younger mice, 22 weeks after excision of the floxed *Rps14* allele, also had impaired differentiation at the RIII–RIV transition ($P < 0.001$) with a decrease in the quiescence of cells in the RI population ($P < 0.001$) (Supplementary Fig. 1f,g). These results suggest that a compensatory increase in erythropoiesis occurs in young *Rps14*-haploinsufficient mice, causing a delay in the development of severe anemia. To determine whether *Rps14* haploinsufficiency in hematopoietic cells but not bone marrow stroma drives anemia, we generated mixed-bone marrow chimeras (Supplementary Fig. 1h). Wild-type (WT) mice transplanted with *Rps14*-haploinsufficient hematopoietic cells developed anemia with kinetics similar to that of untransplanted mice (compare Supplementary Fig. 1h to Fig. 1a), confirming that the phenotype is caused by excision of *Rps14* in hematopoietic cells.

We next examined the effect of *Rps14* haploinsufficiency on stress-induced erythropoiesis, using mice in which hemolysis was induced by phenylhydrazine treatment. After acute hemolytic stress, *Rps14*-haploinsufficient mice developed more severe anemia and had a delayed reticulocyte response, as compared to *Mx1-Cre* control mice (Fig. 1e). The RI population (CD71⁺Ter119⁻) was significantly ($P < 0.001$) increased in frequency in *Rps14^{-/-}Mx1-Cre⁺* mice, whereas the RIV population (CD71^{low}Ter119^{high}) was significantly ($P < 0.001$) decreased in frequency, highlighting a terminal erythroid differentiation defect consistent with

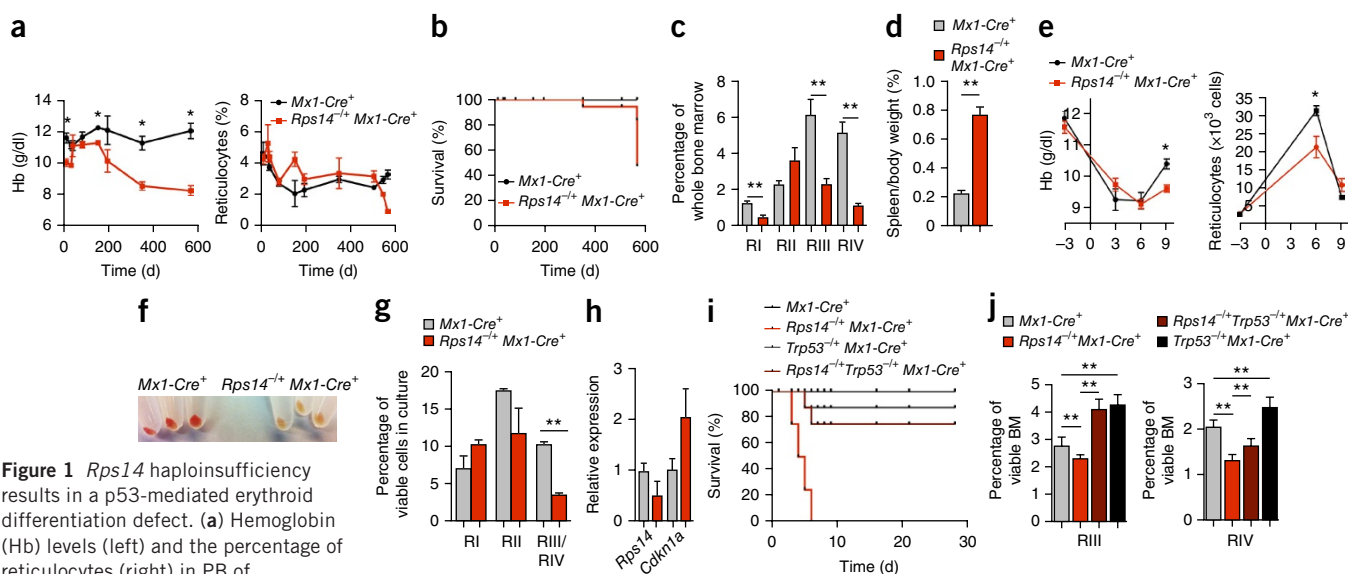


Figure 1 *Rps14* haploinsufficiency results in a p53-mediated erythroid differentiation defect. (a) Hemoglobin (Hb) levels (left) and the percentage of reticulocytes (right) in PB of *Rps14^{-/-}Mx1-Cre⁺* mice in comparison to *Mx1-Cre⁺* WT controls ($n = 10$ per group). (b) Kaplan-Meier survival curves for *Rps14^{-/-}Mx1-Cre⁺* ($n = 10$) and *Mx1-Cre⁺* control ($n = 10$) mice. Time 0 is the day of the first of three poly(I:C) injections. $P = 0.207$; by log-rank test (Mantel-Cox test). (c) Frequency of RI (CD71^{high}Ter119⁻), RII (CD71^{high}Ter119⁺), RIII (RIII: CD71^{intermediate}Ter119⁺) and RIV (CD71^{low}Ter119⁺) erythroid progenitor populations among viable bone marrow cells in *Mx1-Cre⁺* and *Rps14^{-/-}Mx1-Cre⁺* mice 18 months after poly(I:C) treatment ($n = 5$ per group). (d) Relative weight of spleen to total body weight of *Mx1-Cre⁺* and *Rps14^{-/-}Mx1-Cre⁺* mice 18 months after poly(I:C) treatment ($n = 5$ per group). (e) Hb level (left) and reticulocyte counts (right) in PB at serial time points before and after phenylhydrazine injection (25 mg/kg) at day 0 ($n = 8$ per group). (f) Representative image of cell pellets of lineage-negative HSPCs from mice of the indicated genotypes that were subjected to erythroid differentiation *in vitro* for 5 d. (g) Erythroid progenitor populations 5 d after induction of erythroid differentiation ($n = 3$ biological replicates). (h) *Cdkn1a* and *Rps14* transcript levels, as measured by qRT-PCR, in cells 5 d after induction of erythroid differentiation. Data are normalized to expression in *Mx1-Cre⁺* control cells ($n = 5$ biological replicates). (i) Kaplan-Meier survival curves for *Rps14^{-/-}Mx1-Cre⁺*, *p53^{-/-}Mx1-Cre⁺*, *Rps14^{-/-}p53^{-/-}Mx1-Cre⁺* and *Mx1-Cre⁺* control mice ($n = 10$ per group) after treatment with 35 mg/kg phenylhydrazine on two consecutive days (day 0 and day 1). $P < 0.0001$; by log-rank test (Mantel-Cox test). (j) Frequency of RIII and RIV erythroid progenitor populations among viable bone marrow cells in 10- to 12-week-old *Rps14^{-/-}Mx1-Cre⁺* ($n = 14$), *p53^{-/-}Mx1-Cre⁺* ($n = 5$), *Rps14^{-/-}p53^{-/-}Mx1-Cre⁺* ($n = 5$) and *Mx1-Cre⁺* control ($n = 8$) mice, as characterized by differential CD71 and Ter119 expression, 9 d after the first treatment with 25 mg/kg phenylhydrazine. Unless otherwise indicated, data are mean \pm s.d. * $P < 0.05$, ** $P < 0.001$; by unpaired two-sided *t*-test (a–i) or multiple-group comparison (i,j) using analysis of variance (ANOVA) with *post hoc* Tukey correction.

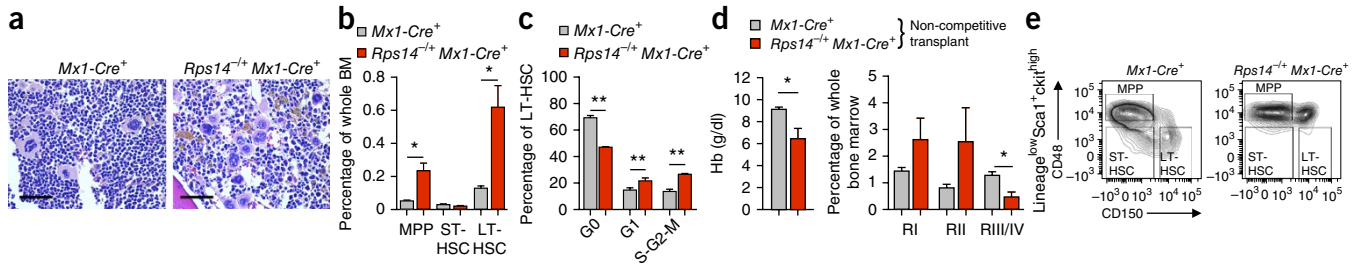


Figure 2 *Rps14* haploinsufficiency affects HSPCs. (a) Representative images of bone marrow histopathology in H&E-stained bone marrow sections (40× magnification) 18 months after the first poly(I:C) injection in *Mx1-Cre*⁺ (*n* = 4) (left) and *Rps14*^{-/-}*Mx1-Cre*⁺ (*n* = 5) (right) mice. Scale bars, 50 μm. (b) Frequency of MPPs (lineage^{low}c-Kit⁺Sca1⁺CD48⁺CD150⁻), ST-HSCs (lineage^{low}c-Kit⁺Sca1⁺CD48⁻CD150⁻) and LT-HSCs (lineage^{low}c-Kit⁺Sca1⁺CD48⁻CD150⁺) 18 months after the first poly(I:C) injection in *Rps14*^{-/-}*Mx1-Cre*⁺ (*n* = 5) and *Mx1-Cre*⁺ (*n* = 4) mice. (c) Cell cycle status of permeabilized LT-HSCs from the bone marrow of mice of the indicated genotypes, as analyzed by staining for the proliferation marker Ki67 and with the DNA dye Hoechst33342 (G0: Ki67⁻Hoechst⁺; G1: Ki67⁺Hoechst⁺; S-G2-M: Ki67⁺Hoechst⁺) (*n* = 5 per group). (d) Hb levels in PB (left) and frequency of RI–RIV erythroid progenitor populations (RI: CD71^{high}Ter119⁻; RII: CD71^{high}Ter119⁺; RIII/IV: CD71^{intermediate/low}Ter119⁺) from chimeric *Rps14*^{-/-}*Mx1-Cre*⁺ mice in comparison to *Mx1-Cre*⁺ chimeric controls 6 weeks after transplantation of cells from whole bone marrow of primary 18-month-old mice of the indicated genotypes into 6- to 8-week-old SJL/CD45.1⁺ recipient mice (*n* = 5 per group). (e) Representative flow cytometry plots of HSPC populations in the bone marrow—defined as MPPs, ST-HSCs and LT-HSCs—in CD45.1⁺ mice transplanted with bone marrow cells from 18-month-old *Mx1-Cre*⁺ (*n* = 4) or *Rps14*^{-/-}*Mx1-Cre*⁺ (*n* = 5) mice 6 weeks after transplantation. (f) Donor chimerism (CD45.2) of *Rps14*^{-/-}*Mx1-Cre*⁺ or *Mx1-Cre*⁺ cells (each mixed in a 50:50 ratio with CD45.1⁺ cells at the time of transplantation) in the peripheral blood. Time 0 indicates when mice were first bled at 4 weeks after transplantation (engraftment) just before inducing the excision of *Rps14* by poly(I:C) injections. After 24 weeks, bone marrow was harvested and transplanted into secondary recipients (*n* = 5 per group). 1st tx, primary transplantation; 2nd tx, secondary transplantation. (g) Donor chimerism (CD45.2) of HSPC populations (MPP, ST-HSC and LT-HSC) in secondary chimeric mice 40 weeks after secondary transplantation (*n* = 5). (h) Hb levels in the PB from chimeric *Rps14*^{-/-}*Mx1-Cre*⁺ and *Mx1-Cre*⁺ mice 64 weeks after engraftment (40 weeks after secondary transplantation) (*n* = 5 per group). Throughout, data are mean ± s.d. **P* < 0.05, ***P* < 0.001; by unpaired two-sided *t*-test.

induction of apoptosis in the RIII (CD71^{intermediate}Ter119⁺) population (Supplementary Fig. 1j). *Rps14*^{-/-}*Mx1-Cre*⁺ mice were characterized by significant splenomegaly with effacement of the normal spleen architecture and expansion of the red pulp (*P* < 0.05; Supplementary Fig. 1i).

To analyze the effect of *Rps14* haploinsufficiency on erythroid differentiation in the absence of *in vivo* compensatory mechanisms, we analyzed erythroid differentiation of lineage-negative hematopoietic stem and progenitor cells (HSPC) *in vitro*. After 5 d of culture, *Mx1-Cre*⁺ HSPCs differentiated into hemoglobinized CD71⁺Ter119⁺ cells, whereas *Rps14*-haploinsufficient cells did not terminally differentiate (Fig. 1f,g). This terminal differentiation defect was accompanied by induction of the expression of *Cdkn1a*, which encodes the p53 downstream-target p21 (Fig. 1h).

The p53 pathway is activated by decreased expression of ribosomal protein genes and has been linked to the erythroid defect in other models of ribosome dysfunction^{7,8,10,13}. We found that compound haploinsufficiency for *Trp53* and *Rps14* prevented mortality from high-dose phenylhydrazine treatment (35 mg per kg body weight (mg/kg); Fig. 1i). After treatment with a lower dose (25 mg/kg), compound haploinsufficiency for *Trp53* normalized the effects on erythropoietic recovery and spleen size caused by *Rps14* haploinsufficiency (Fig. 1j and Supplementary Fig. 1k,l). In aggregate, these results demonstrate that *Rps14* haploinsufficiency causes a *Trp53*-dependent terminal erythroid differentiation defect.

Rps14 haploinsufficiency affects hematopoietic stem and progenitor cells

We next evaluated whether *Rps14* haploinsufficiency affects hematopoiesis more broadly. In a histopathological analysis of the bone marrow,

we found that 18-month-old *Rps14*-haploinsufficient mice had a slightly decreased cellularity, diffuse hemosiderin deposition and substantially increased numbers of hypolobulated micro-megakaryocytes, consistent with the pathognomonic cell morphology of bone marrow biopsies from individuals with del(5q) MDS (Fig. 2a and Supplementary Fig. 2a,b). *Rps14*-haploinsufficient mice had a mild thrombocytosis and platelet dysplasia in peripheral blood (PB) smears (Supplementary Fig. 2c); white blood cell counts (WBC) were normal (Supplementary Fig. 2d). Whereas the HSPC compartment was not altered in young, 22-week-old *Rps14*-haploinsufficient mice (Supplementary Fig. 2e), long-term HSCs (LT-HSCs; lineage^{low}c-Kit⁺Sca1⁺CD48⁻CD150⁺) and multipotent progenitor cells (MPPs; lineage^{low}c-Kit⁺Sca1⁺CD48⁺CD150⁻) were significantly increased in frequency in the bone marrow in *Rps14*-haploinsufficient mice at 18 months of age (Fig. 2b). To analyze whether the expansion of LT-HSCs might be due to exit from quiescence and enhanced LT-HSC cycling, we performed cell cycle analysis. In comparison with *Mx1-Cre*⁺ controls, *Rps14*-haploinsufficient LT-HSCs had a significantly smaller percentage of cells in the G0 phase of cell cycle, and a significantly higher percentage of cells in the G1 and S-G2-M phases, consistent with exit from quiescence (Fig. 2c). Because telomere length reflects the replicative history of a cell, we measured telomere length in bone marrow cells from *Rps14*-haploinsufficient mice and *Mx1-Cre*⁺ control mice. Bone marrow cells from *Rps14*-haploinsufficient mice had significantly shorter telomeres than those from *Mx1-Cre*⁺ control mice (Supplementary Fig. 2i; *P* < 0.001).

We next examined the capacity of HSPCs to reconstitute hematopoiesis following transplantation. We transplanted cells from whole bone marrow of 18-month-old *Rps14*^{-/-}*Mx1-Cre*⁺ and *Mx1-Cre*⁺

control mice into 6- to 8-week-old CD45.1⁺ recipient mice. Mice transplanted with *Rps14*^{-/-}*Mx1-Cre*⁺ bone marrow cells died 6–7 weeks after transplantation and had reduced hemoglobin levels and an erythroid differentiation block from the RII to RIII-IV stage, comparable to the differentiation block observed in the primary (nontransplanted) 18-month-old donor mice (Fig. 2d). Moreover, the transplanted mice had a significant decrease in LT-HSC frequency ($P < 0.05$) and an increase in MPP frequency (although it was not significant) in the bone marrow (Fig. 2e and Supplementary Fig. 2f), but no decrease in the level of bone marrow chimerism (Supplementary Fig. 2g).

Because *Rps14* haploinsufficiency led to a significant increase in LT-HSC frequency in primary, nontransplanted mice, we examined the functional capacity of *Rps14*-haploinsufficient cells in a competitive repopulation assay. We transplanted *Rps14*^{fl/+}*Mx1-Cre*⁺ or *Mx1-Cre*⁺ bone marrow cells in competition with an equal number of age-matched CD45.1⁺ competitor bone marrow cells into lethally irradiated CD45.1⁺ recipient mice (Fig. 2f). Four weeks after transplantation, mice were treated with poly(I:C) to induce heterozygous *Rps14* inactivation. *Rps14*-haploinsufficient cells outcompeted CD45.1⁺ competitor cells in the primary transplant, whereas *Mx1-Cre*⁺ control cells had no competitive advantage (Fig. 2f). To determine long-term repopulation potential, whole-bone marrow cells from primary recipients were transplanted into secondary recipients. In the primary recipients, the contribution of *Rps14*-haploinsufficient bone marrow cells was stable and showed a significantly ($P < 0.05$) higher chimerism than those of *Mx1-Cre*⁺ controls. By 32 weeks after secondary transplantation, we observed a progressive decrease in the bone marrow chimerism of *Rps14*-haploinsufficient bone marrow cells to levels comparable to that of *Mx1-Cre*⁺ control cells (Fig. 2f).

Given the progressive decrease in the chimerism of *Rps14*-haploinsufficient cells, we evaluated the contribution of these cells to different HSPC populations 40 weeks after secondary transplantation. In the multipotent progenitor population, the frequency of *Rps14*-haploinsufficient cells was significantly higher than that of WT cells, whereas no differences were observed in the short-term HSC (ST-HSC; lineage^{low} c-Kit⁺Sca1⁺CD48⁻CD150⁻) and LT-HSC populations (Fig. 2g). In differentiated lineages, we observed significant ($P < 0.05$) myeloid skewing of *Rps14*-haploinsufficient cells, reflected by increased chimerism within the Gr1⁺CD11b⁺ granulocyte population. In contrast, chimerism within lymphoid populations did not differ significantly from that seen with *Mx1-Cre*⁺ control cells (Supplementary Fig. 2h). The chimerism of Ter119⁺ erythroid cells was significantly ($P < 0.05$) decreased in secondary recipients that were transplanted with *Rps14*-haploinsufficient bone marrow (Supplementary Fig. 2h), highlighting the distinct erythroid phenotype. Mice transplanted with equivalent numbers of *Rps14*-haploinsufficient and WT bone marrow cells succumbed to a severe anemia (Fig. 2h) in the setting of relatively preserved whole-blood chimerism (Fig. 2f), suggesting that *Rps14* haploinsufficiency might have cell-extrinsic effects that suppress erythropoiesis.

Taken together, these results indicate that *Rps14* haploinsufficiency causes impaired terminal erythroid differentiation, an increase in HSC frequency with myeloid skewing and age-dependent loss of HSC function. Overall, this hematopoietic phenotype resembles alterations that occur during HSC aging and as a consequence of inflammation in the bone marrow^{16–18}.

Ribosomal haploinsufficiency leads to global reduction in protein synthesis

Having established a mouse model that faithfully recapitulates the cardinal features of del(5q) MDS, we sought to understand how a

heterozygous deletion of *Rps14*, which encodes a component of the 40S ribosomal subunit, alters ribosome assembly and protein synthesis. We first analyzed whether *Rps14* haploinsufficiency induces quantitative changes in protein synthesis by using a fluorogenic assay (O-propargyl-puromycin; OP-puro) to visualize protein synthesis *in vivo*¹⁹. After a single intraperitoneal injection of OP-puro (50 mg/kg), we measured OP-puro incorporation as a reflection of total protein translation in a defined period of time. Overall, OP-puro incorporation was significantly ($P < 0.001$) reduced in *Rps14*^{-/-}*Mx1-Cre*⁺ cells relative to that in WT cells. The reduction in protein synthesis was most striking in erythroid progenitor cells (Fig. 3a and Supplementary Fig. 3a,b), consistent with an erythroid differentiation block and the erythroid cell-specific requirement for high levels of ribosome biogenesis, ribosome activity and protein translation²⁰.

To determine whether the *Rps14* haploinsufficiency specifically affects ribosomal subunit and/or polysome formation, we performed sucrose gradient analysis of intact polysomes from FACS-purified erythroid progenitor cells (lineage^{low}CD71^{high-intermediate}Ter119⁺, from RII to RIII). We observed intact formation of polysome subunits (Fig. 3b), as expected given the rather mild, age-dependent phenotype. These findings indicate that although protein synthesis is impaired, the ribosomes that are assembled function normally. Ribosomal subunits that fail to assemble into an intact 80S ribosome may be rapidly degraded, as previously described^{21–23}.

Ribosomal haploinsufficiency induces increased levels of proteins involved in innate immune function

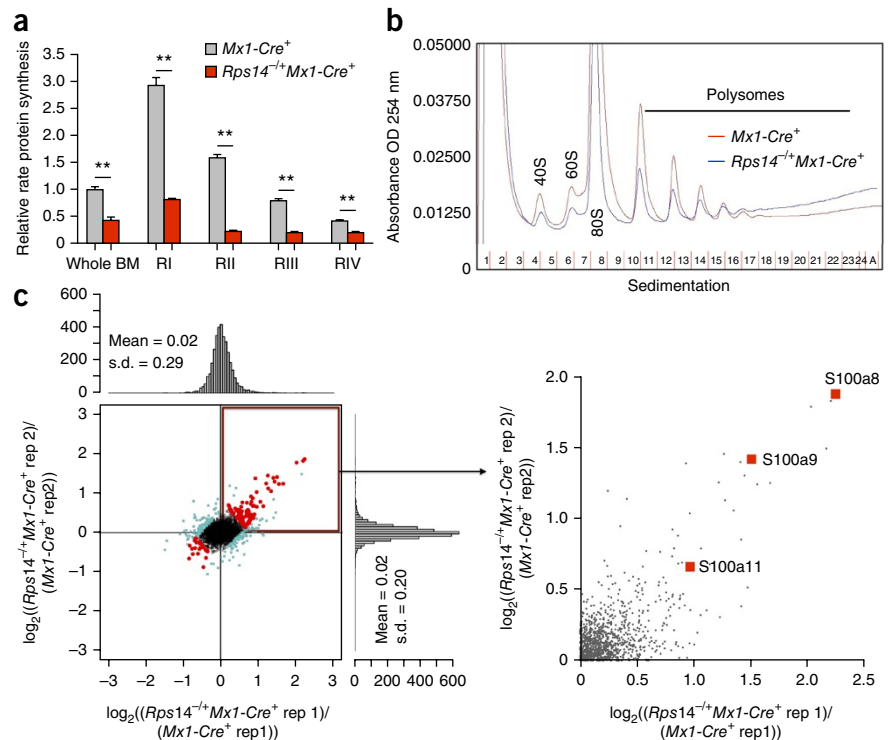
To elucidate a mechanism for the severe erythroid differentiation defect, we performed a quantitative proteomic analysis. We purified erythroid progenitor cells (lineage^{low}CD71^{high-intermediate}Ter119⁺, RII–RIII) and used isobaric tags for relative and absolute quantification (iTRAQ)-based mass spectrometry (Fig. 3c). We detected 3,524 proteins with at least two unique peptides and ratios per replicate. Of these, 26 proteins were differentially expressed (adjusted p -value of < 0.05 ; Supplementary Table 1). Ribosome-associated proteins had decreased expression, consistent with global reduction in protein synthesis, but intact polysome formation (Supplementary Fig. 3c). In *Rps14*-haploinsufficient cells, proteins involved in innate immune system activation, including S100a8 and S100a9, were most enriched. In MDS patients, the S100A9-CD33 pathway and innate immune activation have been implicated in disease pathogenesis^{24,25}.

To validate that *Rps14* haploinsufficiency induces expression of innate immune response proteins, we examined S100a8 expression by immunohistochemistry of the bone marrow of *Rps14*^{-/-} mice and *Mx1-Cre*⁺ control mice (Fig. 4a and Supplementary Fig. 4d). S100a8 expression was higher in bone marrow from *Rps14*-haploinsufficient mice than *Mx1-Cre*⁺ control mice, and distinct clusters of S100A8 expressing cells were observed (Fig. 4a). We confirmed that *S100a8* mRNA and protein expression were increased in lineage-negative bone marrow cells (Fig. 4b). To quantify S100a8 expression in defined cell populations, we simultaneously analyzed surface marker staining and intracellular S100a8 staining. In *Rps14*-haploinsufficient bone marrow cells, S100a8 expression was increased in the erythroid progenitor populations affected by the differentiation block (Gr1⁻CD11b⁻CD71^{high}Ter119^{high} and Gr1⁻CD11b⁻CD71^{low}Ter119^{high}; RIII-RIV population) (Fig. 4c), as well as in monocytes and macrophages (Fig. 4d,e and Supplementary Fig. 4a,b).

Because we observed a rapidly developing anemia in chimeric mice that had been transplanted with aged *Rps14*-haploinsufficient whole-bone marrow cells (Fig. 2), we also analyzed S100a8 expression

Figure 3 Reduced protein synthesis in *Rps14*-haploinsufficient cells. (a) OP-puro fluorescence in whole-bone marrow (BM) cells and erythroid RI–RIV progenitor populations measured 1 h after administration to 20-week-old *Mx1-Cre*⁺ control or *Rps14*^{-/-}*Mx1-Cre*⁺ mice (16 weeks after the first injection of poly(I:C)) (*n* = 5 per group). The results were normalized to those of unfractionated bone marrow in *Mx1-Cre*⁺ mice. Data are mean ± s.d. ***P* < 0.001; by unpaired two-sided *t*-test.

(b) Polysome profiles from sort-purified lineage^{low}CD71^{high}Ter119⁺ erythroid progenitor cells from mice of the indicated genotypes. The x axis shows the distance along the gradient; the y axis shows relative absorbance in arbitrary units. Data are representative of three independent experiments (*n* = 3 biological replicates per experiment). (c) Proteomic analysis of changes in protein expression in lineage^{low}CD71^{high}Ter119⁺ erythroid progenitor cells from *Rps14*^{-/-}*Mx1-Cre*⁺ and *Mx1-Cre*⁺ mice. Left, log₂ ratios of relative protein expression are shown in a scatter plot for individual proteins for replicates 1 (Rep 1, x axis) and 2 (Rep 2, y axis); each dot represents a unique protein. Right, close-up view of the upper right quadrant of the graph on the left (outlined in red), showing proteins that have higher expression in *Rps14*^{-/-}*Mx1-Cre*⁺ relative to *Mx1-Cre*⁺ control cells for replicates 1 and 2. Detailed statistical methods for the proteomic analysis are described in the Online Methods section. Bar graphs show the distribution of the number of proteins detected in replicate 1 (x axis) and replicate 2 (y axis).



in the bone marrow of these chimeric mice. Both monocytes and Gr1⁺CD11b⁺CD71^{low}Ter119^{high} (RIV) erythroblasts from *Rps14*-haploinsufficient mice had dramatically increased expression of S100a8 as compared to those from *Mx1-Cre*⁺ chimeric control mice (Supplementary Fig. 4c; *P* < 0.001). This finding suggests that stress on the bone marrow, such as transplantation or aging, potentiates the expression of S100a8, with consequent effects on hematopoiesis.

The functional unit of mammalian erythropoiesis, the erythroblastic island, consists of a central macrophage that extends cytoplasmic protrusions to a ring of surrounding erythroblasts. Because we found increased S100a8 expression specifically in both erythroblasts and macrophages, we next examined expression of S100a8 and p53 in the erythroblastic island. We performed confocal imaging on cytopins of bone marrow cells from *Rps14*-haploinsufficient and *Mx1-Cre*⁺ mice (Fig. 4d). We found that F4/80⁺ macrophages from *Rps14*-haploinsufficient bone marrow co-expressed S100a8. In close proximity to these macrophages, we detected S100a8-expressing cells, some of which expressed p53, and the numbers of these S100a8-expressing cells was substantially increased in cells from *Rps14*-haploinsufficient bone marrow as compared to those from control bone marrow.

To validate that S100a8 induction leads to p53 expression in erythroid progenitor cells, we analyzed co-expression of p53 and S100a8 in erythroid progenitor cells by flow cytometry (Fig. 4e). In the RIII population, we identified a significant induction of p53 in S100a8-expressing cells. Because p53 is a known regulator of S100a8 (refs. 26–29), we analyzed the expression of S100a8 in *Rps14*-haploinsufficient cells in the presence or absence of p53, both in the steady-state condition (Supplementary Fig. 4e) and during stress-induced erythropoiesis after treatment with phenylhydrazine (Fig. 4f). We detected significantly decreased expression of S100a8 in *Rps14*^{-/-}*Trp53*^{-/-}*Mx1-Cre*⁺

macrophages and RIII erythroid progenitor cells, as compared to that in p53 WT control cells (Fig. 4f and Supplementary Fig. 4e), indicating that induction of p53 by ribosomal haploinsufficiency regulates the expression of S100a8.

Having shown that *Rps14* haploinsufficiency affects not only erythroblasts but also monocytes and macrophages, we measured *S100a8* mRNA expression in purified lineage^{low}CD11b⁺CD71^{high/intermediate}Ter119⁺ (RII–RIII) erythroblasts and in lineage^{low}F4/80⁺ macrophages. For both cell types, *Rps14*-haploinsufficient cells had decreased *Rps14* mRNA expression and increased *S100a8* mRNA expression, as compared to that in *Mx1-Cre*⁺ control cells (Supplementary Fig. 4f; *P* < 0.05 F4/80⁺; *P* < 0.001 RII–RIII). In addition, both *Rps14*-haploinsufficient erythroblasts and macrophages had elevated expression of *Tnfa*, which encodes tumor necrosis factor (TNF)- α , a downstream target of the heterodimeric S100A8–S100A9 complex^{26,30} and a powerful repressor of erythropoiesis^{25,31}. Consistent with impaired erythroid differentiation in *Rps14*-haploinsufficient cells, expression of *Klf1* and *Gata1*, which encode erythroid transcription factors, was decreased.

To investigate whether *Rps14* haploinsufficiency induces an inflammatory environment in the bone marrow that represses erythropoiesis and hematopoiesis by cell-extrinsic mechanisms, we profiled the levels of 40 cytokines in bone marrow serum (Fig. 4g and Supplementary Fig. 4g). We found that levels of four cytokines were significantly increased (*P* < 0.001) in *Rps14*-haploinsufficient mice, as compared to *Mx1-Cre*⁺ control bone marrows—macrophage inflammatory protein (MIP)-1 α (also known as Ccl3), Cxcl9, RANTES (also known as Ccl5), and interleukin (IL)-12(p40). These cytokines are predominantly expressed in activated macrophages and monocytes, have negative effects on erythropoiesis and hematopoiesis, and are

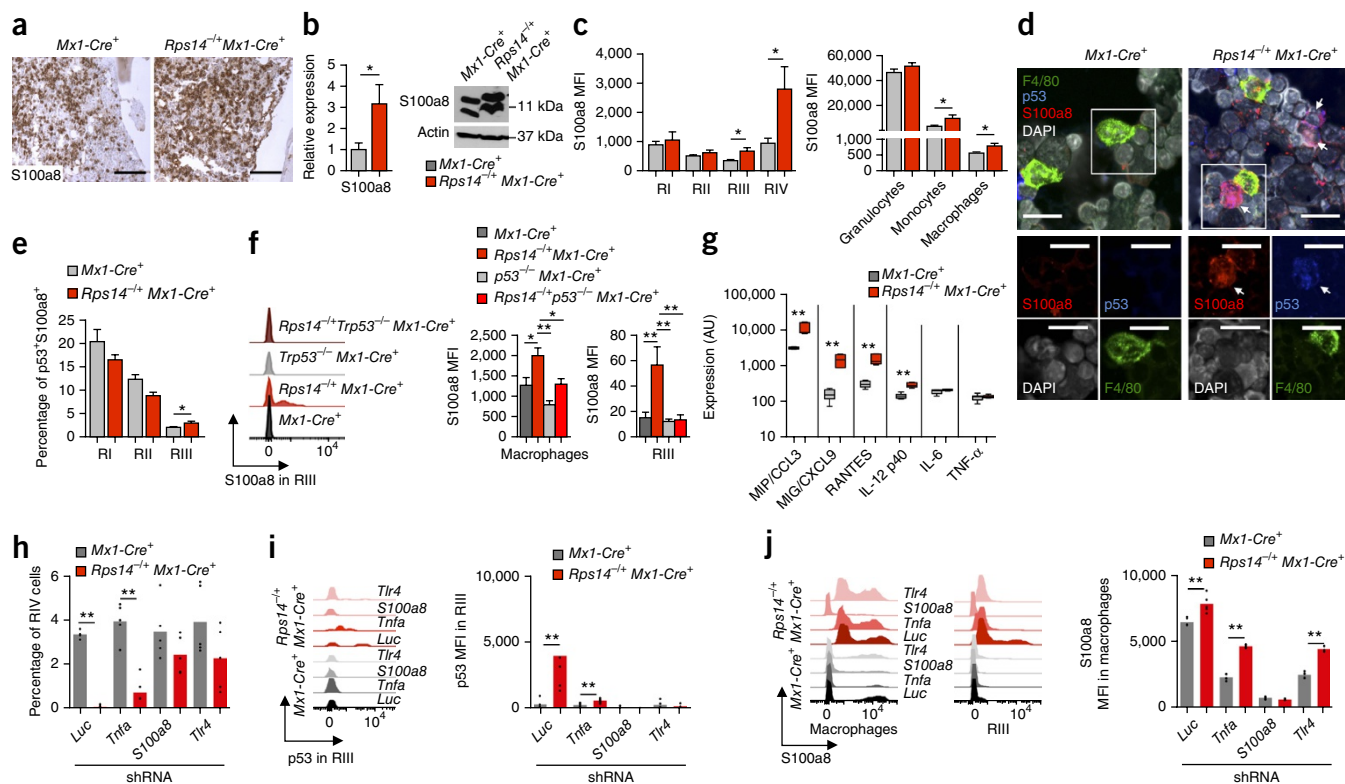


Figure 4 S100a8 is upregulated in bone marrow of *Rps14*-haploinsufficient mice, is regulated by p53 and is necessary for the erythroid differentiation defect. (a) Representative images ($n = 5$) of immunohistochemical staining of S100a8 in bone marrow from *Mx1-Cre*⁺ (left) and *Rps14*^{-/-}*Mx1-Cre*⁺ (right) mice 8 weeks after induction of *Rps14* excision with poly(I:C). Scale bars, 100 μ m. (b) Quantification of S100a8 by qRT-PCR ($n = 5$ per group); data are normalized to expression in *Mx1-Cre*⁺ control cells 8 weeks after poly(I:C) treatment (left) and representative western blot analysis (of three independent experiments) for S100a8 in protein lysates (right) from *Mx1-Cre*⁺ and *Rps14*^{-/-}*Mx1-Cre*⁺ lineage-negative bone marrow cells. Actin was used as a loading control for western blots. (c) S100a8 mean fluorescence intensity (MFI) in CD11b⁺Gr1⁻ erythroid progenitor populations (RI–RIV) ($n = 5$ per genotype) (left) and in Gr1⁺CD11⁺ granulocytes, Gr1⁻CD11⁺ monocytes and F4/80⁺ macrophages ($n = 5$ per genotype) (right) from *Mx1-Cre*⁺ (gray bars) and *Rps14*^{-/-}*Mx1-Cre*⁺ (red bars) mice. (d) Representative images (of three independent experiments) showing co-immunofluorescence staining for F4/80 (green), p53 (dark blue) and S100a8 (red) on cytopins of *Mx1-Cre*⁺ (left) and *Rps14*^{-/-}*Mx1-Cre*⁺ (right) bone marrow cells 12 weeks after induction of *Rps14* excision with poly(I:C). The micrographs on the bottom are magnified images of the white boxed area. Scale bars, 20 μ m (top) and 15 μ m (bottom). (e) Percentage of RI–RIII erythroid progenitor cells from *Rps14*^{-/-}*Mx1-Cre*⁺ and *Mx1-Cre*⁺ mice co-expressing p53 and S100a8 12 weeks after induction of *Rps14* excision with poly(I:C) ($n = 5$). (f) Representative histograms showing S100a8 expression in the RIII population (left) and quantification of S100a8 MFI in F4/80⁺ macrophages and RIII erythroblasts (right) of *Mx1-Cre*⁺, *p53*^{-/-}, *Rps14*^{-/-}*Mx1-Cre*⁺ and *Rps14*^{-/-}*p53*^{-/-}*Mx1-Cre*⁺ mice 6 d after induction of hemolysis with phenylhydrazine treatment ($n = 5$ per group). (g) Fluorescence intensity of the indicated inflammatory cytokines in bone marrow from *Mx1-Cre*⁺ and *Rps14*^{-/-}*Mx1-Cre*⁺ mice 12 weeks after induction of *Rps14* excision with poly(I:C) (log₁₀ scale) ($n = 4$). (h) Frequency of RIV erythroid progenitor populations after transduction of c-Kit⁺ HSPCs with five individual lentiviral shRNAs targeting *Tnfa*, *S100a8* or *Tlr4*, as well as a control shRNA targeting the luciferase gene (*Luc*), selection with puromycin and induction of cells to undergo erythroid differentiation for 5 d *in vitro* ($n = 3$). Circles represent the median of three replicates for each individual shRNA (five independent shRNAs per gene). The mean value for the five shRNAs targeting a given gene is shown with a gray or red bar. (i) Representative histograms showing p53 expression (left) and quantification of p53 MFI (right) in the RIII population of HSPCs that were transduced with shRNAs targeting *Tnfa*, *S100a8* or *Tlr4* and the *Luc* control and differentiated for 5 d *in vitro* to allow erythroid differentiation ($n = 3$ mice per group). Circles represent the median of three replicates for each individual shRNA. The mean value for the five shRNAs targeting a given gene is shown with a gray or red bar. (j) Representative histograms showing S100a8 expression in F4/80⁺ macrophages (left) and the RIII population (middle) and quantification of S100a8 MFI in macrophages (right) of HSPCs treated as in i ($n = 3$ mice per group). Circles represent the median of three replicates for each individual shRNA. The mean value for the five shRNAs targeting a given gene is shown with a gray or red bar. Throughout, data are mean \pm s.d.

* $P < 0.05$, ** $P < 0.001$; by unpaired two-sided *t*-test (b,c,e,h–j) or multiple-group comparison by ANOVA with *post hoc* Tukey correction (f).

substantially elevated in patients with low-risk MDS^{32–35}. Recent studies have demonstrated that S100A8 and S100A9 are endogenous activators of Toll-like receptor 4 (TLR4) (ref. 36). We found that *Tlr4* expression was increased on both macrophages and monocytes, but not on erythroblasts, in the bone marrow of *Rps14*-haploinsufficient mice (Supplementary Fig. 4h; $P < 0.05$), suggesting that S100a8 activates macrophages and monocytes and contributes to an inflammatory environment.

We examined the roles of S100a8, *Tlr4* and TNF- α in causing abnormal erythropoiesis in *Rps14*-haploinsufficient cells using

validated shRNAs (Supplementary Fig. 4i). We transduced c-Kit⁺ HSPCs with test and control shRNAs, induced erythroid differentiation *in vitro* and evaluated the effects by using flow cytometry and hemoglobinization assays (Fig. 4h and Supplementary Fig. 4j). Knockdown of *S100a8* or *Tlr4* improved erythroid differentiation and reduced p53 induction (Fig. 4i), indicating that *S100a8* and *Tlr4* are central to the erythropoietic defect of *Rps14* haploinsufficiency. *Tnfa* knockdown had a similar, although less robust, effect on erythropoiesis and had no effect on *S100a8* expression (Fig. 4i,j), suggesting a pro-inflammatory role downstream of that of S100a8.

S100a8 is necessary and sufficient for the erythroid-differentiation defect of *Rps14* haploinsufficiency

To explore a cell non-autonomous mechanism by which S100a8 causes an erythroid differentiation defect, we induced erythroid differentiation of WT lineage-negative HSPCs in the presence of recombinant S100a8 protein (rS100a8). HSPCs cultured in the presence of rS100a8 had a differentiation block at the RIII-RIV

transition (Fig. 5a and Supplementary Fig. 5a), consistent with the differentiation defect observed in *Rps14*-haploinsufficient cells, with significantly increased p53 expression in the RII-RIII population (Fig. 5b).

We next used CRISPR-Cas9 technology to genetically inactivate *S100a8* and test the requirement for S100a8 in the erythroid differentiation defect caused by *Rps14* haploinsufficiency.

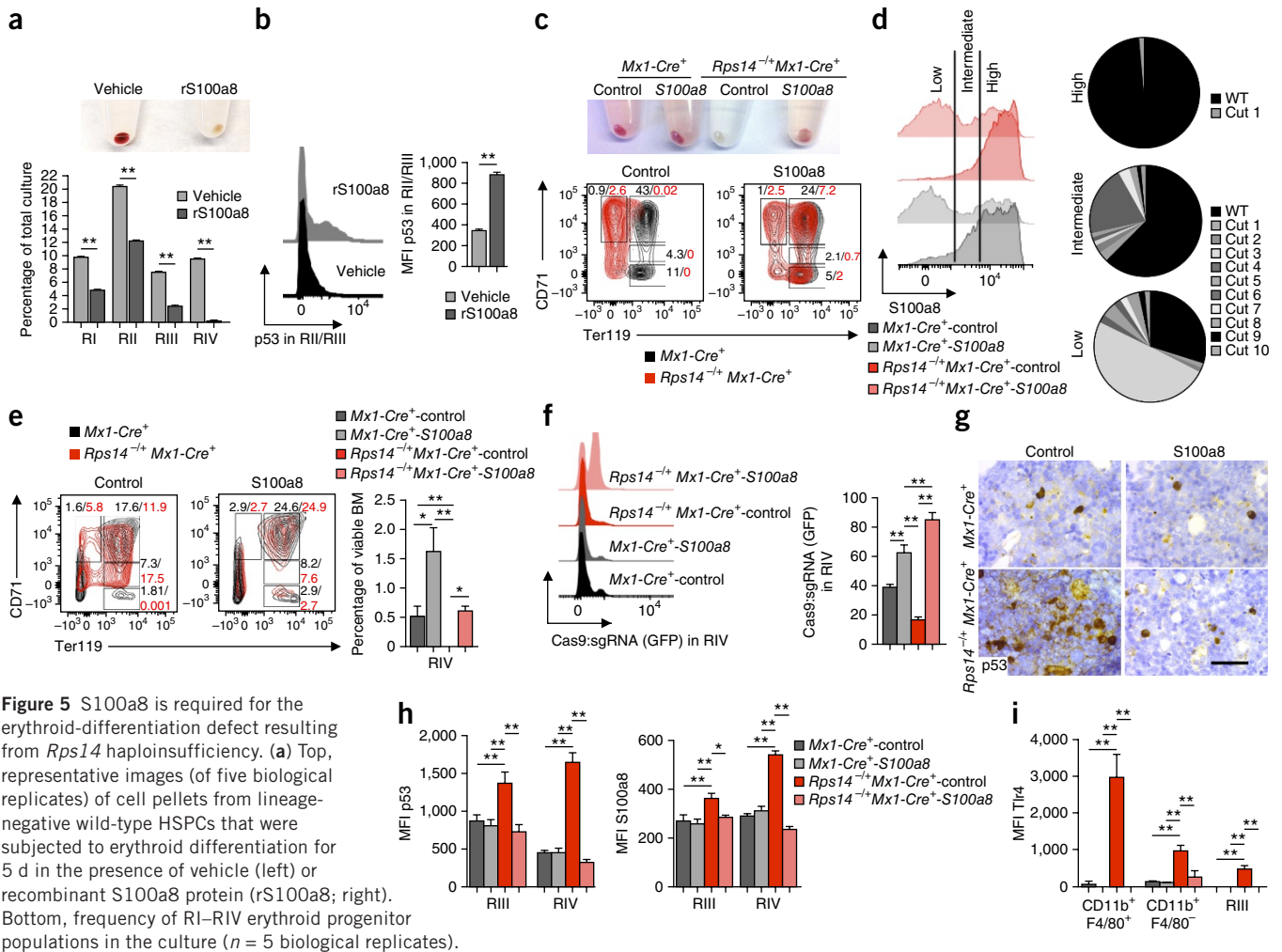


Figure 5 S100a8 is required for the erythroid-differentiation defect resulting from *Rps14* haploinsufficiency. (a) Top, representative images (of five biological replicates) of cell pellets from lineage-negative wild-type HSPCs that were subjected to erythroid differentiation for 5 d in the presence of vehicle (left) or recombinant S100a8 protein (rS100a8; right). Bottom, frequency of RI–RIV erythroid progenitor populations in the culture ($n = 5$ biological replicates).

(b) Representative histograms for intracellular flow cytometry analysis (left) and quantification (right) of p53 expression in the RII and RIII populations of HSPCs after 5 d of erythroid differentiation *in vitro* in the presence or absence of recombinant S100a8 ($n = 5$ biological replicates).

(c) Representative images of cell pellets of c-Kit⁺ HSPCs from *Rps14*^{-/-}*Mx1-Cre*⁺ or *Mx1-Cre*⁺ mice expressing *S100a8*-specific or control sgRNAs after erythroid differentiation *in vitro* (top) and representative flow cytometry plots of the erythroid progenitor populations characterized by CD71 and Ter119 expression (RI–RIV) (bottom) (data are representative of $n = 3$ biological replicates).

(d) Left, representative histograms of S100a8 expression in Gr1^{low}CD11b⁺ monocytes from *Rps14*^{-/-}*Mx1-Cre*⁺ or *Mx1-Cre*⁺ HSPCs that had been transduced with either *S100a8*-specific or control sgRNAs and differentiated *in vitro* for 5 d. Right, pie charts depicting the relative representation of wild-type (WT) sequence or unique insertions or deletions (cut 1–cut 10) detected at the genomic target site—sorted on the basis of high, intermediate and low S100a8 expression—in cells transduced with the *S100a8*-specific sgRNA:Cas9 construct.

(e) Phenylhydrazine was injected in chimeric WT mice to induce hemolysis 6 weeks after transplantation with c-Kit⁺ HSPCs from *Rps14*^{-/-}*Mx1-Cre*⁺ or *Mx1-Cre*⁺ mice; the HSPCs had been transduced with a lentiviral vector expressing Cas9 and either an sgRNA targeting *S100a8* or a control sgRNA. Left, representative flow plots of the RI–RIV erythroid progenitor populations 6 d after the first dose of phenylhydrazine. Right, frequency of the RIV population in the bone marrow 6 d after the first dose of phenylhydrazine ($n = 5$ per group).

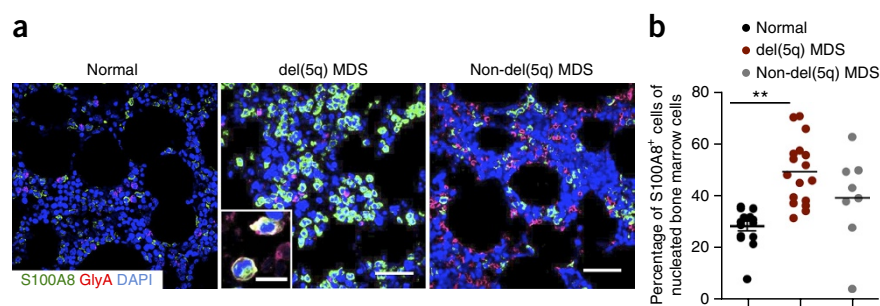
(f) In chimeric mice as in **e**, representative histograms of GFP expression in the RIV population in bone marrow 6 d after the first dose of phenylhydrazine (left), and frequency of GFP⁺ cells in the RIV population 6 d after the first dose of phenylhydrazine (right) ($n = 5$ per group).

(g) Representative image of immunostaining for p53 in bone marrow from chimeric WT mice transplanted with *Mx1-Cre*⁺ (top) or *Rps14*^{-/-}*Mx1-Cre*⁺ (bottom) HSPCs transduced with either control (left) or *S100a8*-specific (right) sgRNA:Cas9 6 d after the first dose of phenylhydrazine. Scale bar, 50 μ m.

(h) Quantification of p53 (left) and S100a8 (right) MFI in RIII and RIV populations of bone marrow from *Rps14*^{-/-}*Mx1-Cre*⁺ or *Mx1-Cre*⁺ mice transduced with either control or *S100a8*-specific sgRNA:Cas9 6 d after treatment with phenylhydrazine ($n = 5$ per group).

(i) Quantification of Tlr4 MFI in macrophages (CD11b⁺F4/80⁺), monocytes (CD11b⁺F4/80⁻) and erythroid progenitors (RIII) in bone marrow from *Rps14*^{-/-}*Mx1-Cre*⁺ or *Mx1-Cre*⁺ mice transduced with either control or *S100a8*-specific sgRNA:Cas9 6 d after the first dose of phenylhydrazine ($n = 5$ per group). Throughout, data are mean \pm s.d. * $P < 0.05$, ** $P < 0.001$; by unpaired two-sided *t*-test (**a, b**) or multiple-group comparison (**e–i**) using ANOVA with *post hoc* Tukey correction.

Figure 6 S100A8⁺ cell frequency is increased in bone marrow from individuals with del(5q) MDS. **(a)** Representative images of immunofluorescence staining for glycoprotein A (GlyA, magenta), S100A8 (green) and DAPI (blue, nuclear stain) in healthy individuals (normal; $n = 15$), patients with del(5q) MDS ($n = 21$) and subjects with normal-karyotype MDS (non-del(5q) MDS; $n = 9$). The inset depicts cells that co-express S100A8 and GlyA. Scale bars, 100 μm and 10 μm (inset). Micrographs for all individuals are shown in **Supplementary Figure 6**. **(b)** Quantification of S100A8⁺ cells as a percentage of DAPI⁺, nucleated bone marrow cells (healthy (normal) individuals, $n = 15$; patients with del(5q) MDS, $n = 21$; subjects with normal-karyotype MDS (non-del(5q) MDS), $n = 9$). Data are mean \pm s.d. $**P < 0.001$; by unpaired two-sided t -test.



We transduced c-Kit⁺ HSPCs with a lentiviral vector expressing the Cas9 nuclease and a small guide RNA (sgRNA) targeting *S100a8* and then analyzed erythroid differentiation *in vitro*. Compared to control nontargeting sgRNA (NTG-sgRNA:Cas9), CRISPR-mediated inactivation of *S100a8* (using S100a8-sgRNA:Cas9) in *Rps14*-haploinsufficient cells rescued the terminal differentiation of hemoglobinized RIV erythroid cells (**Fig. 5c**). We confirmed efficient introduction of frameshift insertion and deletion mutations in, and reduced protein-level expression of, *S100a8* in myeloid and erythroid cells (**Fig. 5d** and **Supplementary Fig. 5c**).

We next determined whether *S100a8* is necessary for the erythroid-differentiation defect caused by *Rps14* haploinsufficiency *in vivo* after phenylhydrazine-induced hemolysis (**Fig. 5e–i**). We transplanted HSPCs expressing either S100a8-sgRNA:Cas9 or control NTG-sgRNA:Cas9 into lethally irradiated WT recipients, which were treated with phenylhydrazine 6 weeks after transplantation. In contrast to the control, S100a8-sgRNA:Cas9 expression in *Rps14*^{+/-}*Mx1-Cre*⁺ hematopoietic cells rescued the ablation of the RIV population (**Fig. 5e** and **Supplementary Fig. 5e,f**), leading to a marked positive selection of Cas9:sgRNA-GFP⁺ RIV cells (**Fig. 5f**), a reduced induction of p53 and S100a8 in erythroid cells (**Fig. 5g,h** and **Supplementary Fig. 5g**), a decreased frequency of Tlr4-expressing macrophages (**Fig. 5i** and **Supplementary Fig. 5d,e,g**) and a reduced induction of TNF- α (**Supplementary Fig. 5h**). These data demonstrate the functional requirement for S100a8 in the induction of a p53-dependent erythroid-differentiation defect and an increase in the frequency of Tlr4-expressing macrophages in the setting of *Rps14* haploinsufficiency.

To examine cell-intrinsic effects of S100a8 in *Rps14*-haploinsufficient cells, we purified RII erythroblasts and measured the effect of S100a8 inactivation on their terminal differentiation, in the absence of myeloid cells (**Supplementary Fig. 5i**). Purified *Rps14*-haploinsufficient RII progenitor cells expressing a control sgRNA did not terminally differentiate and underwent apoptosis, whereas those expressing S100a8-sgRNA:Cas9 differentiated into hemoglobinized, terminally differentiated erythroid cells. These data indicate that S100a8 directly affects erythroid progenitor cells by intrinsic mechanisms.

Next, to examine potential cell-extrinsic effects of S100a8, we analyzed S100a8 and p53 induction in competitive transplant studies, in both WT competitor cells (CD45.1⁺) and in *Rps14*^{+/-}*Mx1-Cre*⁺ or *Mx1-Cre*⁺ (CD45.2⁺) cells (**Supplementary Fig. 5j**). Induction of S100a8 expression was restricted to CD45.2⁺ *Rps14*-haploinsufficient cells as compared to WT competitor (CD45.1⁺) ($P < 0.001$) or *Mx1-Cre*⁺ cells ($P < 0.05$). In contrast, induction of p53 expression occurred in CD45.1⁺ competitor cells only after they were mixed with CD45.2⁺

Rps14-haploinsufficient cells and not in the presence of *Mx1-Cre*⁺ cells ($P < 0.05$). This finding is consistent with the idea that increased S100a8 expression in *Rps14*-haploinsufficient cells exerts a pro-apoptotic effect on WT cells that may drive progressive anemia in a cell-extrinsic fashion, even in the setting of preserved whole-bone marrow chimerism. Taken together, these data demonstrate that S100a8 exerts both cell-intrinsic and cell-extrinsic effects on erythropoiesis.

The frequency of S100A8⁺ cells in del(5q) MDS human bone marrow positively correlates with disease severity

To examine whether ribosomal haploinsufficiency leads to activation of S100A8 in individuals with del(5q) MDS, we performed immunofluorescence for S100A8 and the erythroid marker glycoprotein A (GlyA) in bone marrow biopsies from non-MDS control individuals (normal) and MDS patients with and without the del(5q) lesion (**Fig. 6**, **Supplementary Fig. 6a,b** and **Supplementary Table 2**). In biopsies from normal individuals (control), rare S100A8-expressing cells were interspersed in the hematopoietic marrow. In biopsies from individuals with del(5q) MDS, S100A8⁺ cells were positioned in the marrow in groups of >5 cells. The frequency of S100A8-expressing nucleated cells was substantially increased in bone marrow biopsies from subjects with del(5q) MDS as compared to those from normal individuals (**Supplementary Fig. 6b**). GlyA⁺ early erythroid progenitor cells occasionally co-expressed S100A8 (**Fig. 6a**, inset), similarly to what was observed in the *Rps14*-haploinsufficient mouse model. In aggregate, these data indicate that impaired erythropoiesis in the bone marrow of patients with del(5q) MDS is associated with aberrant expression of S100A8.

DISCUSSION

Anemia is the most common hematologic manifestation of MDS, particularly in patients with del(5q) MDS. In a newly generated conditional-knockout mouse model of *Rps14*, we found that *Rps14* haploinsufficiency is sufficient to cause a p53-dependent erythroid-differentiation defect, associated with apoptosis, that results in age-dependent progressive anemia, megakaryocyte dysplasia and loss of HSC quiescence. In an unbiased proteomic analysis, we identified a link between *Rps14* haploinsufficiency and induction of the danger-associated molecular pattern (DAMP) heterodimer S100a8-S100a9 in monocytes, macrophages and erythroblasts. Our studies link the p53-dependent erythroid-differentiation defect to induction of S100a8 and an inflammatory environment to which both monocytes and macrophages contribute, and we demonstrate that ribosomal haploinsufficiency exerts both cell-intrinsic and cell-extrinsic effects on erythropoiesis and hematopoiesis.

S100A8-S100A9 expression is induced during inflammatory processes including infection, autoimmunity, and cancer^{26,36,37}. In addition to granulocytes and macrophages, which produce these proteins under steady-state conditions, other cell types induce S100A8-S100A9 expression in response to stress³⁰. As a consequence of *Rps14* haploinsufficiency, S100a8 expression was induced in both CD11b⁺ monocytes and F4/80⁺ macrophages, as well as in late-stage erythroblasts, and induction of S100a8 in erythroblasts was associated with increased p53 expression. Our data indicate that disruption of regulatory mechanisms in the erythroblastic island, in which erythroid progenitor cells interact with a central macrophage, contributes to the erythroid-differentiation defects observed in the bone marrow of *Rps14*-haploinsufficient mice. S100A9 activation has been described in MDS patient samples^{24,38}, and the S100A9-CD33 pathway in myeloid-derived suppressor cells (MDSCs) perturbs hematopoiesis²⁴. On the basis of our data, we posit that the S100A8 and S100A9 proteins—which are induced as a stress response by ribosomal haploinsufficiency in monocytes, macrophages and erythroblasts—contribute to the MDS phenotype.

The S100A8-S100A9 heterodimer, an endogenous TLR4 ligand, acts upstream of TNF- α and promotes the activation of the transcription factor NF- κ B and the secretion of pro-inflammatory cytokines³⁷. Consistent with this previous work, our data demonstrate that in the setting of *Rps14* haploinsufficiency, S100a8 acts upstream of Tlr4 and TNF- α in contributing to the erythroid-differentiation defect. *RPS14* and microRNA 145 (*MIR145*) are always co-deleted in the 5q- syndrome, and both converge mechanistically on TLR4 signaling^{25,39–43}, highlighting potential cooperative and additive effects of genes that affect the same downstream pathways on the 5q- syndrome (Supplementary Fig. 7).

S100 proteins participate in an autoregulatory feedback loop with p53, serving both as upstream drivers of *Trp53* gene transcription and as direct downstream p53 transcriptional targets^{26–29}. Consistent with these reports, we found that p53 is required for induction of S100a8 expression in *Rps14*-deleted cells and that adding recombinant S100a8 is sufficient to induce p53 activity in erythroid progenitor cells, leading to a block in terminal erythroid differentiation.

Specific cytokines are elevated in the serum of individuals with MDS³³, and these inflammatory signals can alter the proliferation and apoptosis of MDS HSPCs^{44,45}. Indeed, chronic immune stimulation, coupled with senescence-dependent changes⁴⁶ in both HSPCs and the bone marrow microenvironment⁴⁷, may be central to the pathogenesis of MDS^{25,40,48}. Our analysis of *Rps14*-deleted HSCs suggests that inflammatory cues that are induced by *Rps14* haploinsufficiency impact HSC aging and quiescence^{17,18,42,49}. In patients with chronic inflammation, cytokines in the bone marrow have been associated with inhibition of erythropoiesis⁵⁰. In particular, TNF- α expression has been implicated in the erythroid defects observed in patients with DBA³¹, and it is upregulated in the bone marrow serum of patients with MDS^{51,52}. Moreover, TNF receptor-associated factor 6 (TRAF6) activation, a process targeted by miR-145 and miR-146a, induces myelodysplasia in a mouse model²⁵.

Our data link haploinsufficiency of a ribosomal gene, *Rps14*, with the activation of S100A8-S100A9 and other inflammatory molecules and the inhibition of erythropoiesis. An intervention that blocks this process, potentially through pharmacologic targeting of S100A8-S100A9, could improve red blood cell production in individuals with del(5q) MDS. These findings underscore a molecular link between the genetic abnormalities in patients with MDS, activation of the innate immune system and the ineffective hematopoiesis that characterizes the disease.

METHODS

Methods and any associated references are available in the [online version of the paper](#).

Accession codes. The original mass spectra may be downloaded from [MassIVE](#) using the identifier [MSV000079482](#). The data are accessible at <ftp://massive.ucsd.edu/MSV000079482>.

Note: Any Supplementary Information and Source Data files are available in the online version of the paper.

ACKNOWLEDGMENTS

This work was supported by the US National Institutes of Health (NIH) (grant no. R01HL082945; B.L.E.), a Gabrielle's Angel Award (B.L.E.), a Leukemia and Lymphoma Society Scholar and Specialized Center of Research (SCOR) award (B.L.E.), the German Research Foundation (DFG1188/3-1; R.K.S.), a Max Eder fellowship provided by the German Cancer Aid (Deutsche Krebshilfe, grant no. 111750; R.K.S.), the Edward P. Evans Foundation (R.K.S.) and the German Cluster of Excellence program Regenerative Biology to Reconstructive Therapy (REBIRTH; to G.B.). We thank D. Haase (Georg-August-Universität Göttingen) for the cytogenetic (karyotype) analysis in individuals with del(5q) MDS. This work was supported by the confocal microscope facility, a core facility of the Interdisciplinary Center for Clinical Research (Interdisziplinäres Zentrum für klinische Forschung; IZKF) Aachen, within the Faculty of Medicine at RWTH Aachen University.

AUTHOR CONTRIBUTIONS

R.K.S., R.C.L., S.A.C. and B.L.E. designed experiments; R.K.S., M.S., R. Kramann, M.V.F., C.E.J., C.H., F.B., M.C.C., E.C., C.S.W., C.D.N. and L.P.C. performed experiments and analyzed data; F.B., T.H.B., U.G., U.P., R. Knüchel and G.B. collected patient samples and clinical information, reviewed bone marrow biopsies and analyzed data; R.K.S. and B.L.E. wrote the manuscript; and all authors provided critical reviews of the manuscript.

COMPETING FINANCIAL INTERESTS

The authors declare no competing financial interests.

Reprints and permissions information is available online at <http://www.nature.com/reprints/index.html>.

- Ebert, B.L. Deletion 5q in myelodysplastic syndrome: a paradigm for the study of hemizygous deletions in cancer. *Leukemia* **23**, 1252–1256 (2009).
- Ebert, B.L. Molecular dissection of the 5q deletion in myelodysplastic syndrome. *Semin. Oncol.* **38**, 621–626 (2011).
- Komrokji, R.S., Padron, E., Ebert, B.L. & List, A.F. Deletion 5q MDS: molecular and therapeutic implications. *Best Pract. Res. Clin. Haematol.* **26**, 365–375 (2013).
- Ebert, B.L. *et al.* Identification of *RPS14* as a 5q- syndrome gene by RNA interference screen. *Nature* **451**, 335–339 (2008).
- Choesmel, V. *et al.* Impaired ribosome biogenesis in Diamond-Blackfan anemia. *Blood* **109**, 1275–1283 (2007).
- Ruggero, D. & Shimamura, A. Marrow failure: a window into ribosome biology. *Blood* **124**, 2784–2792 (2014).
- McGowan, K.A. *et al.* Ribosomal mutations cause p53-mediated dark skin and pleiotropic effects. *Nat. Genet.* **40**, 963–970 (2008).
- McGowan, K.A. *et al.* Reduced ribosomal protein gene dosage and p53 activation in low-risk myelodysplastic syndrome. *Blood* **118**, 3622–3633 (2011).
- Matsson, H. *et al.* Erythropoiesis in the *Rps19*-disrupted mouse: analysis of erythropoietin response and biochemical markers for Diamond-Blackfan anemia. *Blood Cells Mol. Dis.* **36**, 259–264 (2006).
- Dutt, S. *et al.* Haploinsufficiency for ribosomal protein genes causes selective activation of p53 in human erythroid progenitor cells. *Blood* **117**, 2567–2576 (2011).
- Pellagatti, A. *et al.* Induction of p53 and upregulation of the p53 pathway in the human 5q- syndrome. *Blood* **115**, 2721–2723 (2010).
- Zhou, X., Hao, Q., Liao, J., Zhang, Q. & Lu, H. Ribosomal protein S14 unties the MDM2-p53 loop upon ribosomal stress. *Oncogene* **32**, 388–396 (2013).
- Barlow, J.L. *et al.* A p53-dependent mechanism underlies macrocytic anemia in a mouse model of human 5q- syndrome. *Nat. Med.* **16**, 59–66 (2010).
- Raiser, D.M., Narla, A. & Ebert, B.L. The emerging importance of ribosomal dysfunction in the pathogenesis of hematologic disorders. *Leuk. Lymphoma* **55**, 491–500 (2014).
- Volarevic, S. *et al.* Proliferation but not growth blocked by conditional deletion of 40S ribosomal protein S6. *Science* **288**, 2045–2047 (2000).
- Morrison, S.J., Wandycz, A.M., Akashi, K., Globerson, A. & Weissman, I.L. The aging of hematopoietic stem cells. *Nat. Med.* **2**, 1011–1016 (1996).

17. Pang, W.W. *et al.* Human bone marrow hematopoietic stem cells are increased in frequency and myeloid-biased with age. *Proc. Natl. Acad. Sci. USA* **108**, 20012–20017 (2011).
18. Du, W. *et al.* Inflammation-mediated notch signaling skews Fanconi anemia hematopoietic stem cell differentiation. *J. Immunol.* **191**, 2806–2817 (2013).
19. Signer, R.A., Magee, J.A., Salic, A. & Morrison, S.J. Haematopoietic stem cells require a highly regulated protein synthesis rate. *Nature* **509**, 49–54 (2014).
20. Lajtha, L.G. & Oliver, R. A kinetic model of the erythron. *Proc. R. Soc. Med.* **54**, 369–371 (1961).
21. Karbstein, K. Inside the 40S ribosome assembly machinery. *Curr. Opin. Chem. Biol.* **15**, 657–663 (2011).
22. Strunk, B.S. & Karbstein, K. Powering through ribosome assembly. *RNA* **15**, 2083–2104 (2009).
23. Strunk, B.S. *et al.* Ribosome assembly factors prevent premature translation initiation by 40S assembly intermediates. *Science* **333**, 1449–1453 (2011).
24. Chen, X. *et al.* Induction of myelodysplasia by myeloid-derived suppressor cells. *J. Clin. Invest.* **123**, 4595–4611 (2013).
25. Starczynowski, D.T. *et al.* Identification of miR-145 and miR-146a as mediators of the 5q- syndrome phenotype. *Nat. Med.* **16**, 49–58 (2010).
26. Bresnick, A.R., Weber, D.J. & Zimmer, D.B. S100 proteins in cancer. *Nat. Rev. Cancer* **15**, 96–109 (2015).
27. Li, C. *et al.* A novel p53 target gene, *S100A9*, induces p53-dependent cellular apoptosis and mediates the p53 apoptosis pathway. *Biochem. J.* **422**, 363–372 (2009).
28. Tan, M., Heizmann, C.W., Guan, K., Schafer, B.W. & Sun, Y. Transcriptional activation of the human *S100A2* promoter by wild-type p53. *FEBS Lett.* **445**, 265–268 (1999).
29. Mueller, A. *et al.* The calcium-binding protein S100A2 interacts with p53 and modulates its transcriptional activity. *J. Biol. Chem.* **280**, 29186–29193 (2005).
30. Hiratsuka, S., Watanabe, A., Aburatani, H. & Maru, Y. Tumor-mediated upregulation of chemoattractants and recruitment of myeloid cells predetermines lung metastasis. *Nat. Cell Biol.* **8**, 1369–1375 (2006).
31. Bibikova, E. *et al.* TNF-mediated inflammation represses GATA1 and activates p38 MAP kinase in *RPS19*-deficient hematopoietic progenitors. *Blood* **124**, 3791–3798 (2014).
32. Schepers, K. *et al.* Myeloproliferative neoplasia remodels the endosteal bone marrow niche into a self-reinforcing leukemic niche. *Cell Stem Cell* **13**, 285–299 (2013).
33. Kordasti, S.Y. *et al.* IL-17-producing CD4⁺ T cells, pro-inflammatory cytokines and apoptosis are increased in low-risk myelodysplastic syndrome. *Br. J. Haematol.* **145**, 64–72 (2009).
34. Su, S. *et al.* Inhibition of immature erythroid progenitor cell proliferation by macrophage inflammatory protein-1 α by interacting mainly with a C-C chemokine receptor, CCR1. *Blood* **90**, 605–611 (1997).
35. Frisch, B.J. *et al.* Functional inhibition of osteoblastic cells in an *in vivo* mouse model of myeloid leukemia. *Blood* **119**, 540–550 (2012).
36. Vogl, T. *et al.* Mrp8 and Mrp14 are endogenous activators of Toll-like receptor 4, promoting lethal, endotoxin-induced shock. *Nat. Med.* **13**, 1042–1049 (2007).
37. Ehrchen, J.M., Sunderkötter, C., Foell, D., Vogl, T. & Roth, J. The endogenous Toll-like receptor 4 agonist S100A8-S100A9 (calprotectin) as an innate amplifier of infection, autoimmunity and cancer. *J. Leukoc. Biol.* **86**, 557–566 (2009).
38. Wei, Y. *et al.* Global H3K4me3 genome mapping reveals alterations of innate immunity signaling and overexpression of *JMJD3* in human myelodysplastic syndrome CD34⁺ cells. *Leukemia* **27**, 2177–2186 (2013).
39. Chang, K.H. *et al.* p62 is required for stem cell–progenitor retention through inhibition of IKK–NF- κ B–Ccl4 signaling at the bone marrow macrophage–osteoblast niche. *Cell Rep.* **9**, 2084–2097 (2014).
40. Starczynowski, D.T. & Karsan, A. Deregulation of innate immune signaling in myelodysplastic syndromes is associated with deletion of chromosome arm 5q. *Cell Cycle* **9**, 855–856 (2010).
41. Starczynowski, D.T. *et al.* *TRAF6* is an amplified oncogene bridging the RAS and NF- κ B pathways in human lung cancer. *J. Clin. Invest.* **121**, 4095–4105 (2011).
42. Reynaud, D. *et al.* IL-6 controls leukemic multipotent progenitor cell fate and contributes to chronic myelogenous leukemia development. *Cancer Cell* **20**, 661–673 (2011).
43. Rhyasen, G.W. *et al.* Targeting IRAK1 as a therapeutic approach for myelodysplastic syndrome. *Cancer Cell* **24**, 90–104 (2013).
44. Kristinsson, S.Y. *et al.* Chronic immune stimulation might act as a trigger for the development of acute myeloid leukemia or myelodysplastic syndromes. *J. Clin. Oncol.* **29**, 2897–2903 (2011).
45. Takizawa, H., Boettcher, S. & Manz, M.G. Demand-adapted regulation of early hematopoiesis in infection and inflammation. *Blood* **119**, 2991–3002 (2012).
46. Verschoor, C.P. *et al.* Blood CD33⁺HLA-DR⁻ myeloid-derived suppressor cells are increased with age and a history of cancer. *J. Leukoc. Biol.* **93**, 633–637 (2013).
47. Raaijmakers, M.H. *et al.* Bone progenitor dysfunction induces myelodysplasia and secondary leukaemia. *Nature* **464**, 852–857 (2010).
48. Fang, J. *et al.* Cytotoxic effects of bortezomib in myelodysplastic syndrome–acute myeloid leukemia depend on autophagy-mediated lysosomal degradation of TRAF6 and repression of PSMA1. *Blood* **120**, 858–867 (2012).
49. Rossi, D.J. *et al.* Deficiencies in DNA damage repair limit the function of hematopoietic stem cells with age. *Nature* **447**, 725–729 (2007).
50. Means, R.T. Jr. Pathogenesis of the anemia of chronic disease: a cytokine-mediated anemia. *Stem Cells* **13**, 32–37 (1995).
51. Sawanobori, M. *et al.* Expression of TNF receptors and related signaling molecules in the bone marrow from patients with myelodysplastic syndromes. *Leuk. Res.* **27**, 583–591 (2003).
52. Jacobs-Helber, S.M. *et al.* Tumor necrosis factor–alpha expressed constitutively in erythroid cells or induced by erythropoietin has negative and stimulatory roles in normal erythropoiesis and erythroleukemia. *Blood* **101**, 524–531 (2003).

ONLINE METHODS

Generation of *Rps14* conditional-knockout mice and mouse experiments.

The *Rps14* target region is 2.12 kb and includes exons 2–4. Briefly, a 10.64-kb region that was used to construct the targeting vector was first subcloned from a positively identified C57BL/6 BAC (bacterial artificial chromosome) clone (RP23: 205B18). The region was designed such that the 5' homology arm extends about 5.76 kb 5' to the single *LoxP* site. The 3' homology arm ends 3' to the *loxP*- and FRT-flanked neomycin (Neo) cassette and is 2.76 kb long. The *loxP*- and FRT-flanked Neo cassette was inserted 255 bp downstream of exon 4. The single *loxP* site, containing engineered ApaI and Bcl I sites for Southern blot analysis, was inserted 379 bp upstream of exon 2. The targeting vector was confirmed by restriction site analysis after each modification step. P6 and T7 primers anneal to the backbone vector sequence and were used to read into the 5' and 3' ends of the BAC subclone. N1 and N2 primers anneal to the 5' and 3' ends of the *LoxP*-FRT-Neo cassette and were used to sequence the short homology arm (SA) and long homology arm (LA), respectively. The BAC was subcloned into a ~2.4-kb backbone vector (pSP72, Promega) containing an ampicillin selection cassette for retransformation of the construct before electroporation. A pGK-gb2 *loxP*-FRT-Neo cassette was inserted into the gene. The targeting construct was linearized using NotI before electroporation into embryonic stem (ES) cells. The total size of the targeting construct (including vector backbone and Neo cassette) is 14.74 kb. Targeted iTL ICI1 (C57BL/6N) embryonic stem cells were microinjected into BALB/c blastocysts. Resulting chimeras with a high percentage of black coat color were mated to wild-type C57BL/6N mice to generate F1 heterozygous offspring. Tail DNA was analyzed from pups with black coat color. PCR was performed to detect the presence of the distal *LoxP* site using 'LEVI 3' (5'-GTGATCTCAACGCAGGTGTGTAGC-3') and 'SDL2' (5'-TAACAGCATGGAAGTCGGGTCTCA-3') primers. This reaction amplifies a wild-type product 474 bp in size. The presence of a second PCR product 73 bp larger in size than the wild-type product indicates the presence of a distal *LoxP* site.

Chimeric mice were generated by standard methods. The Neo cassette was deleted by crossing the mice with transgenic FLP1 recombinase mice purchased from Jackson Lab (Strain: B6.Cg-Tg(ACTFLPe)9205Dym/J). Chimeric mice were genotyped by PCR with primers reverse (5'-GTGATCTCAACGCAGGTGTGTAGC-3') and forward (5'-TAACAGCATGGAAGTCGGGTCTCA-3') using the following parameters: 95 °C for 3 min, followed by 35 cycles of 95 °C for 30 s, 60 °C for 1 min and 72 °C for 1 min. Following confirmation of germline transmission, mice were crossed with the *Mx1-Cre* mouse strain (Jackson: 002527). To excise *Rps14* exon 2–4, 6- to 8-week-old *Rps14* conditional mice (and *Mx1-Cre*⁺ mice as controls) were given three rounds of 200 µg poly(I:C) (GE Healthcare Life Sciences) using intraperitoneal injections. Excision after Cre recombination was confirmed by PCR with primers to detect a floxed portion of the construct (NdeI 2: 5'-GTATCTCCAATGGTCAGCAATCACGG-3' and LEVI: 5'-GTGATCTCAACGCAGGTGTGTAGC-3'). The sizes of the PCR products from the floxed and WT alleles are 511 and 623 bp, respectively. For qRT-PCR, the *Rps14*-specific Taqman probe mCG6028 was used in a Taqman expression Assay (Assay ID Mm00849906_g1; Life Technologies # 4331182). *Rps14*-haploinsufficient mice were further bred to *p53*-null mice (Jackson stock number 00813). Animals were monitored two to three times a week for the presence of disease by general inspection and palpation. Peripheral blood was collected from the retro-orbital cavity using an EDTA-treated glass capillary and automated total and differential blood cell counts were determined using a Hemavet 950 instrument (Drew Scientific). Following sacrifice, mice were examined for the presence of abnormalities, and organs were collected for further cell and histopathological analysis. Due to the experimental design, the genotypes of the mice could not be blinded or randomized. The group size was chosen based on our experience with conditional mouse knockout models of genes on 5q in order to detect a disease-typical fold change as significant⁵³. All groups of mice (experimental and control mice) were age- and sex-matched. Mouse experiments were performed according to an Institutional Animal Care and Use Committee (IACUC)-approved protocol at Children's Hospital Boston.

Flow cytometry and cell isolation. Bone marrow cells were isolated by flushing and crushing the pelvis, hind leg bones and vertebrae, using a mortar and

pestle, in PBS (GIBCO) supplemented with 2% heat-inactivated FBS (FBS) and penicillin-streptomycin (GIBCO). Whole bone marrow was lysed on ice with red blood cell (RBC) lysis solution (Invitrogen/Life Technologies) and washed in PBS (GIBCO) with 2% FBS. Single-cell suspensions of spleen were prepared by pressing tissue through a 70-µm cell strainer followed by red blood cell lysis. Cells were labeled with monoclonal antibodies in 2% FBS–PBS for 30 min on ice. For flow cytometric analysis and isolation of specific hematopoietic progenitors, cells were incubated with combinations of antibodies to the following cell surface markers (conjugated to FITC, phycoerythrin (PE), allophycocyanin (APC), PercP-Cy5.5, APC-Cy7 (APC-efluor780), Pe-Cy7, Alexa Fluor 700, Pacific blue (efluor450) or biotin): CD3 (17A2), CD5 (53-7.3), CD11b (M1/70), Gr1 (RB6-8C5), B220 (RA3-6B2), Ter119 (TER119), CD71 (C2), c-Kit (2B8), Sca1 (D7), CD34 (RSM34), CD16/32 (93), CD150 (TC15-12F12.2), CD48 (HM48-1), CD45.1 (A20), CD45.2 (104). For sorting of lineage-negative cells, lineage markers included CD3, CD5, CD11b, Gr1 and Ter119. For sorting of erythroid progenitor cells, the lineage cocktail did not include Ter119. All reagents were acquired from BD Biosciences, eBiosciences, or BioLegend. To increase the sorting efficiency, whole-bone marrow samples were either lineage-depleted or c-Kit-enriched using paramagnetic microbeads and an autoMACS magnetic separator (Miltenyi Biotec). Cell sorting was performed on a FACSAria flow cytometer (BD Biosciences); data acquisition was performed on an LSR II or Canto II instrument (BD Biosciences). Data were analyzed by FlowJo (Tree Star) software.

Long-term competitive repopulation assays. In competitive bone marrow transplantation studies, 2×10^6 freshly isolated bone marrow cells were transplanted in competition with 2×10^6 freshly isolated CD45.1⁺ bone marrow cells, via tail vein injection, into female lethally irradiated (10.5 Gy) 6- to 8-week-old CD45.1⁺ recipient mice. Donor cell chimerism was determined in the peripheral blood 4 weeks after transplantation before the excision of *Rps14* was induced by poly(I:C) injection (week 0) as well as every 4–8 weeks. Red blood cells were lysed (Invitrogen/Life Technologies) and the remaining cells were stained with antibodies against CD45.2, CD45.1, Gr1, CD11b, CD3, and CD19 (eBio1D3) to assess donor cell engraftment. For secondary transplants, 5×10^6 bone marrow cells collected from primary recipients were transplanted into lethally irradiated CD45.1⁺ recipient mice.

In vivo measurement of protein synthesis. One hundred microliters of a 20 mM solution of O-propargyl-puromycin (OP-puro; Life Technologies) was injected intraperitoneally; mice injected with PBS were used as controls. Bone marrow and spleen were harvested after 1 hour and then kept on ice. 3×10^6 cells were stained with antibodies against cell surface markers, fixed in 1% paraformaldehyde, and permeabilized in PBS with 3% FBS and 0.1% saponin. An azide-alkyne cyclo-addition was performed using the Click-iT Cell Reaction Buffer Kit (Life Technologies) and an azide-derived dye (conjugated to Alexa Fluor 488; Life Technologies) at 5 µM final concentration for 30 min. Cells were washed twice again and then analyzed by flow cytometry. 'Relative rates of protein synthesis' were calculated by normalizing OP-Puro signals to whole bone marrow after subtracting background auto-fluorescence, as described by Singer *et al.*¹⁹.

Methylcellulose assays. 48 h after viral transduction, 15,000 c-Kit⁺ cells were sorted and plated in semisolid methylcellulose culture medium (M3434, StemCell Technologies) and incubated at 37 °C in a humidified atmosphere. Colony formation was assessed 7 d after plating.

shRNA and sgRNA:CRISPR-Cas9 vector construction, virus production and transduction. Lentivirally expressed shRNAs in the pLKO.1 backbone vector (puromycin resistance) were obtained from the RNAi Consortium at the Broad Institute. The *S100A8*-specific guide RNA (gRNA; forward 5'-CACCGAATTGTG GTAGACATCAATG-3'; reverse 5'-AAACCATTGATGTCTACCACAATTC-3') was cloned into pL-CRISPR.EFS.GFP (<http://www.addgene.org/57827>) using BsmBI restriction digestion. Lentiviral particles were produced by transient transfection of 293T cells with lentivirus plasmid together with pSPAX and VSVG packaging plasmids using TransIT-LT (Mirus). Lentiviral particles were concentrated using ultracentrifugation. c-Kit⁺ or lineage-negative cells were cultured in StemSpan SFEM (StemCell Technologies) supplemented with

50 ng/ml murine thrombopoietin (ThPO) and 50 ng murine stem cell factor (SCF) (both Peprotech) for 24 h and then transduced with concentrated lentiviral supernatant in the presence of 2 µg/ml Polybrene using spin-infection for 90 min at 2,200 r.p.m. at 37 °C.

Sequencing analysis of CRISPR variants. To assess the proportion and diversity of CRISPR variants, we performed PCR-amplicon deep sequencing of bulk genomic DNA at the *S100a8* sgRNA target site (chr3:90669574-90669596; mm9 genome build) using the primers S100a8-g1-F: 5'-GGACACTCAGTAGTGACCATTT-3' and S100a8-g1-R: 5'-GAGTAACTGCAGCTCCCATC-3'. After addition of sample indexes and sequencing adaptors, the product was subjected to 150-nt paired-end sequencing on an Illumina MiSeq instrument, producing approximately 100,000 reads per sample. Reads were then aligned to the genomic reference and grouped according to specific insertion and deletion sequences.

In vitro erythroid differentiation. Total bone marrow cells were labeled with biotin-conjugated anti-lineage antibodies, consisting of anti-CD3e, anti-CD11b, anti-CD45R-B220, anti-Ly6G-Ly6C and anti-TER-119 (BD Pharmingen, San Diego, CA) and purified using anti-biotin beads and negative selection on an autoMACS instrument (Miltenyi Biotec). Purified cells were then seeded in fibronectin-coated (2 µg/cm²) tissue culture-treated polystyrene wells (BD Discovery Labware, Bedford, MA) at a cell density of 1 × 10⁵ per ml. Erythroid differentiation was carried out according to modified, published protocols⁵⁴. The erythropoietic medium consisted of Iscove's modified Dulbecco's medium (IMDM; Gibco) supplemented with erythropoietin (EPO) at 10 units/ml, 10 ng/ml SCF (Peprotech), 10 µM dexamethasone (Sigma), 15% FBS, 1% detoxified BSA, 200 µg/ml holotransferrin (Sigma, St. Louis, MO), 10 µg/ml recombinant human insulin (Sigma), 2 mM L-glutamine, 10⁻⁴ M β-mercaptoethanol and penicillin-streptomycin. After 48 h the medium was replaced by maintenance medium consisting of IMDM with 20% FBS, 2 mM L-glutamine and 10⁻⁴ M β-mercaptoethanol. Recombinant S100a8 (mouse, Abnova P4345) protein was used where indicated, at a concentration of 1 µg/ml.

Phenylhydrazine treatment. Phenylhydrazine was purchased from Sigma and injected subcutaneously at two consecutive days (days 0 and 1) at a dose of 35 or 25 mg/kg, as previously described⁵⁵. Peripheral blood was collected 4 d before the start of treatment and at days 3, 6 and 9 after initial injection. Phenylhydrazine treatment experiments were carried out in 8- to 12-week-old mice. All groups of mice (experimental and control mice) were age- and sex-matched.

Polysome profiling. For polysome profiling of primary erythroid progenitor cells, whole bone marrow was lineage-depleted (CD3, CD5, B220, Gr1, and CD11b) using microbeads and the autoMACS instrument as described above and stained for Ter119 and CD71. Erythroid progenitor cells (lineage⁻CD71^{high}Ter119^{intermediate/high}) were sort-purified in 100% FCS and cultured for 1 h in IMDM with 20% FCS and 2 mM L-glutamine at 37 °C under humidified conditions. Cells (approximately 3 × 10⁶) were then harvested, spun down and incubated with 100 µg/ml cycloheximide for 10 min at 37 °C, washed with ice-cold PBS containing 100 µg/ml cycloheximide and lysed in 300 µl of a solution containing 5 mM Tris (pH 7.4), 2.5 mM MgCl₂ and 1.5 mM KCl. Gradients were poured using a Biocomp Gradient Station. Polysomes were separated on a 10–50% linear sucrose gradient containing 20 mM HEPES-KOH (pH 7.4), 5 mM MgCl₂, 100 mM KCl, 2 mM DTT and 100 µg/ml cycloheximide and centrifuged at 36,000 r.p.m. for 2 h in a Beckman Coulter L8-M centrifuge with a SW40Ti rotor. Gradients were fractionated using a Gilson FC-203B fractionator. Absorbance at 254 nm was used to visualize the gradients using a BioRad EM-1 Econo UV monitor.

iTRAQ labeling of peptides and basic reversed-phase (brp) fractionation. 20 million RII and RIII erythroblasts (four biological replicates per one technical or process replicate) were sort-purified and resuspended in 500 µl lysis buffer (8 M urea, 50 mM Tris HCl, 1 mM EDTA, 75 mM NaCl, aprotinin, leupeptin, PMSF, NaF, proteinase inhibitor cocktails 2 and 3; all Sigma), vortexed on ice and spun at 20,000g for 10 min at 4 °C. 300 µg protein of each sample was reduced (2 µl 500 mM DTT, 30 min, RT), alkylated (4 µl 500 mM iodoacetic acid, 45 min, dark) and digested using 2 µg of sequencing-grade trypsin

overnight with shaking at room temperature (**Supplementary Table 3**). The samples were then quenched and desalted on 10 mg SepPak columns. Desalted peptides were labeled with iTRAQ reagents according to the manufacturer's instructions (AB Sciex, Foster City, CA). Peptides were dissolved in 30 µl 0.5 M TEAB pH 8.5 solution (Sigma-Aldrich) and labeling reagent was added in 70 µl of ethanol. After a 1-h incubation, the reaction was stopped with 50 mM Tris-HCl pH 7.5. Differentially labeled peptides were mixed and subsequently desalted on a 30 mg SepPak column. Basic reversed-phase fractionation and subsequent concatenation of the differentially labeled and combined peptides was performed as described by Mertins *et al.*⁵⁶ with the following amendment: the Zorbax 300-Å extended C18 column used was 2.1 × 150 mm with a 3.5-µm bead size (Agilent).

Mass spectrometry analysis. Reconstituted peptides were separated on an online nanoflow EASY-nLC 1000 UHPLC system (Thermo Fisher Scientific) and analyzed on a benchtop Orbitrap Q Exactive mass spectrometer (Thermo Fisher Scientific). The peptide samples were injected onto a capillary column (Picofrit with 10-µm tip opening and 75-µm diameter, New Objective, PF360-75-10-N-5) packed in-house with 20 cm C18 silica material (1.9-µm ReproSil-Pur C18-AQ medium, Dr. Maisch GmbH, r119.aq). The UHPLC setup was connected with a custom-fit microadapting tee (360 µm, IDEX Health & Science, UH-753), and capillary columns were heated to 50 °C in column heater sleeves (Phoenix-ST) to reduce backpressure during ultra-high pressure liquid chromatography (UHPLC) separation. Injected peptides were separated at a flow rate of 200 nL/min with a linear 80-min gradient from 100% solvent A (3% acetonitrile, 0.1% formic acid) to 30% solvent B (90% acetonitrile, 0.1% formic acid), followed by a linear 6-min gradient from 30% solvent B to 90% solvent B. Each sample was run for 120 min, including sample loading and column equilibration times. The Q Exactive instrument was operated in the data-dependent mode acquiring higher-energy collisional dissociation tandem mass spectrometry (HCD MS/MS) scans ($R = 17,500$) after each MS1 scan ($R = 70,000$) on the 12 most abundant ions using an MS1 ion target of 3×10^6 ions and an MS2 target of 5×10^4 ions. The maximum ion time used for the MS/MS scans was 120 ms; the HCD-normalized collision energy was set to 27; the dynamic exclusion time was set to 20 s, and the peptide-match and isotope-exclusion functions were enabled.

Quantification and identification of peptides and proteins. All mass spectra were processed using the Spectrum Mill software package v4.2 pre-release (Agilent Technologies), which includes modules developed by us for iTRAQ-based quantification. Precursor ion quantification was done using extracted ion chromatograms (XIC's) for each precursor ion. The peak area for the XIC of each precursor ion subjected to MS/MS was calculated automatically by the Spectrum Mill software in the intervening high-resolution MS1 scans of the liquid chromatography coupled to tandem mass spectrometry (LC-MS/MS) runs using narrow windows around each individual member of the isotope cluster. Peak widths in both the time and m/z domains were dynamically determined based on MS-scan resolution, precursor charge and m/z , subject to quality metrics on the relative distribution of the peaks in the isotope cluster versus theoretical distribution. Similar MS/MS spectra acquired on the same precursor m/z in the same dissociation mode within ± 60 s were merged. MS/MS spectra with precursor charge >7 and poor quality MS/MS spectra, which failed the quality filter by not having a sequence tag length >1 (i.e., a minimum of three masses separated by the in-chain mass of an amino acid) were excluded from searching. For peptide identification, MS/MS spectra were searched against the mouse Uniprot database to which a set of common laboratory contaminant proteins was appended. Search parameters included: ESI-QEXACTIVE-HCD scoring parameters, trypsin enzyme specificity with a maximum of two missed cleavages, 40% minimum matched peak intensity, ± 20 p.p.m. precursor-mass tolerance, ± 20 p.p.m. product-mass tolerance, and carbamidomethylation of cysteines, iTRAQ labeling of lysines and peptide N termini as fixed modifications. Allowed variable modifications were oxidation of methionine, N-terminal acetylation, pyroglutamic acid (N-termQ), deamidated (N), pyro-carbamidomethyl, Cys (N-termC), with a precursor MH⁺ shift range of -18 Da to 64 Da. Identities interpreted for individual spectra were automatically designated as valid by optimizing score and delta rank1-rank2 score thresholds separately for each precursor charge state in each LC-MS/MS, while allowing a

maximum target decoy-based false-discovery rate (FDR) of 1.0% at the spectrum level. In calculating scores at the protein level and reporting the identified proteins, redundancy was addressed in the following manner: the protein score is the sum of the scores of distinct peptides. A distinct peptide is the single highest-scoring instance of a peptide detected through an MS/MS spectrum. MS/MS spectra for a particular peptide may have been recorded multiple times (i.e., as different precursor-charge states, isolated from adjacent brp fractions, and modified by oxidation of methionine), but which are still counted as a single distinct peptide. When a peptide sequence >8 residues long is contained in multiple protein entries in the sequence database, the proteins are grouped together and the highest-scoring one and its accession number are reported. In some cases in which the protein sequences are grouped in this manner, there are distinct peptides which uniquely represent a lower-scoring member of the group (isoforms or family members). Each of these instances spawns a subgroup, in which case multiple subgroups are reported and counted toward the total number of proteins. iTRAQ ratios were obtained from the protein-comparisons export table in Spectrum Mill. To obtain iTRAQ protein ratios, the median was calculated over all distinct peptides assigned to a protein subgroup in each replicate⁵⁷. To assign differentially expressed proteins, we used the Limma package in the R environment to calculate moderated *t*-test *P*, as described previously. We also added Blandt-Altman testing to filter out proteins for which the confidence interval for reproducibility was below 95%. Normalized iTRAQ ratios for the two biological replicates were filtered to retain only those deemed reproducible. Reproducible replicates were then subjected to a moderated *t*-test to assess statistical significance. This statistic is similar to the ordinary *t*-statistic, with the exception that standard errors are calculated using an empirical Bayes method using information across all proteins, thereby making inference about each individual protein more robust. The nominal *P* values arising from the moderated *t*-statistic were corrected for multiple-testing by controlling the false-discovery rate (FDR), as proposed by Benjamini and Hochberg. Proteins with an FDR-adjusted *P* < 0.01 were deemed to be reproducibly regulated. Statistical significance was assessed using only reproducible data points.

Cytokine array. To detect inflammatory cytokines in bone marrow serum, we applied the mouse Inflammation Array G1 (CODE: AAM-INF-G1, 8-sample size) according to the manufacturer's instructions. For detection of TNF- α in the bone marrow serum, we used the TNF- α quantikine ELISA assay (R&D Systems). The long bones of mice were kept on ice and flushed with a total of 200 μ l pure (100%) PBS. Cell-serum suspensions were spun down twice at 4 °C at 2,200 r.p.m., and the supernatant was harvested and then spun at 13,000 r.p.m. for 10 min. Protein content was determined using the Pierce protein content BCA assay kit; 100 μ g protein in 100 μ l was used per sample.

Western blots. Western blots were performed according to standard protocols. In brief, cell lysis was performed in RIPA buffer (Pierce) with protease and phosphatase inhibitors. After protein quantification, lysates (Pierce) were resuspended in Laemmli sample buffer and loaded onto gradient gels (Criterion Tris-HCl Gel, 8–16%). Proteins were transferred onto Immobilon polyvinylidene difluoride (PVDF) membranes. Primary antibodies to S100A8 (Abcam ab92331; 1:500), Rps14 (Abcam ab199273; 1:500) and actin (Abcam EPR8484; 1:10,000) were used. Blots were incubated with HRP-conjugated secondary antibody and developed using SuperSignal West Pico Chemiluminescent Substrate (Pierce).

Histopathology, immunohistochemistry and immunofluorescence. For histological and immunohistochemical analyses, organs and bones were fixed in 3.7% formaldehyde overnight, dehydrated and prepared for paraffin embedding. Hematoxylin-eosin (H&E) staining was done according to routine protocols. For immunohistochemical staining, the avidin-biotin complex (ABC)-horse radish peroxidase (HRP) (Dako Cytomation, K5001) was applied for color development using an Autostainer platform (Dako Cytomation, Glostrup, Denmark). Peripheral-blood smears were stained with May-Grünwald-Giemsa (Sigma-Aldrich). For immunofluorescence studies, sternum sections were fixed in 4% paraformaldehyde on ice for 1 h, then incubated in 30% sucrose in PBS at 4 °C overnight. Cytospins were air-dried

first and then fixed in 4% paraformaldehyde for 10 min at room temperature. OCT-embedded (Sakura Finetek) tissues were cryosectioned into 7- μ m-thick sections and mounted on Superfrost slides (Fisher Scientific). For immunofluorescence staining, sections were washed in 1 \times PBS, blocked in 10% normal goat serum (Vector Labs) and incubated with primary antibodies specific for S100A8 (Abcam ab92331), p53 (Cell Signaling, 1C12) or CD68 (DAKO, clone PGM1). Secondary antibodies were conjugated to FITC, Cy3, or Cy5 (Jackson ImmunoResearch). Nuclei were then stained with DAPI (4', 6'-diamidino-2-phenylindole) and mounted in Prolong Gold (Life Technologies). Images were obtained on a Nikon Eclipse E400 microscope (Nikon, Tokyo, Japan) equipped with a SPOT RT color digital camera model 2.1.1 (Diagnostic Instruments) or obtained on a confocal microscope (Nikon C1 eclipse, Nikon, Melville, NY).

Confocal quantitative fluorescent *in situ* hybridization (Q-FISH) staining. Deparaffinization and antigen retrieval of paraffin-embedded bone marrow specimens was carried out using standard protocols. Telomere Q-FISH staining was performed as described previously^{58–60}. Briefly, telomeres were stained with Cy3-(C3TA2) PNA (Panagene, South Korea) followed by six further washing steps, and DNA staining was performed using DAPI (Sigma, USA). All images of bone marrow sections were captured within 48 h after the samples were processed and stored at 4 °C. Telomere length analysis was performed using an LSM710 confocal microscope (Zeiss, Jena, Germany). Images were captured using 63 \times optical magnification with an additional 1.2 \times digital zoom; a multi-tracking mode on 0.5- μ m steps was used to acquire images after staining with DAPI and Cy3. Maximum projection of five single consecutive steps was done, and the acquired images were used for further digital-image analysis. Five representative images of randomly chosen areas were captured for each bone marrow sample. Telomere length detection was carried out using Definiens software (Definiens, Germany). Nuclei and telomeres were detected based on DAPI and Cy3 intensity.

Primary human samples and confocal microscopy. Patient samples originated from different study centers in Germany; this study was approved by institutional review boards at the University of Technology Dresden, Heinrich-Heine-University Düsseldorf, and University Hospital RWTH Aachen. Samples were de-identified at the time of inclusion. All patients provided informed consent, and the data collection was performed in accordance with the Declaration of Helsinki. Criteria for inclusion of del(5q) MDS patients were: cytogenetic isolated del(5q), blast counts <5% in the bone marrow and International Prognostic Scoring System (IPSS) of low risk or intermediate-1. Patient data are summarized in **Supplementary Table 1**. Bone marrow biopsies were fixed for 24 h using the Hannover Solution (12% buffered formaldehyde plus 64% methanol), decalcified (15% EDTA), dehydrated and embedded in paraffin. For immunofluorescence, samples were deparaffinized, hydrated using a decreasing ethanol series and subjected to heat-induced antigen retrieval using citrate buffer pH 6.0, before proceeding to immunofluorescence co-staining. Sections were first blocked with 1 \times Roti-block (Carl Roth, Karlsruhe, Germany) for 1 h at RT, washed with PBS-Tween permabilizing reagent and then incubated at 4 °C overnight with primary rabbit monoclonal anti-S100A8 antibody (Abcam, ab92331, 1:250). After completion of the washing steps, sections were incubated for 30 min at RT with goat anti-rabbit secondary antibody Alexa Fluor 488 conjugate (Life Technologies, Darmstadt, A-11034). Sections were then incubated at 4 °C overnight with primary mouse monoclonal anti-glycophorin A antibody (Dako, M0819, 1:50) or anti-MPO (DAKO, A0398, 1:300) followed by incubation for 30 min at RT with donkey anti-mouse secondary antibody (Alexa Fluor 633- or Alexa Fluor 555-conjugated, Life Technologies, Darmstadt). Nuclei were stained with DAPI and mounted with Vectashield mounting medium (Vector Labs, CA, USA). All antibodies were diluted in 0.1 \times Roti-block. Fluorescence was acquired with a confocal laser scanning microscope (LSM 710, Zeiss, Germany) running Zen 2012 software (Zeiss). A 405-nm diode laser (DAPI) and a 488 nm–633 nm argon laser (Alexa Fluor 488–Alexa Fluor 633) were used for fluorescence excitation. Maximal-intensity projections of three z-stacks of 1- μ m thickness each were acquired. Quantification of S100A8 in nucleated cells was done using ImageJ open source software.

Statistical analysis. Data are presented as mean \pm s.d. Comparison of two groups was performed using an unpaired *t*-test. For multiple-group comparisons, analysis of variance (ANOVA) with *post hoc* Tukey correction was applied. Statistical analyses were performed using GraphPad Prism 5.0c (GraphPad Software Inc., San Diego, CA). *P* < 0.05 was considered significant.

53. Sahin, E. *et al.* Telomere dysfunction induces metabolic and mitochondrial compromise. *Nature* **470**, 359–365 (2011).
54. Schneider, R.K. *et al.* Role of casein kinase 1A1 in the biology and targeted therapy of del(5q) MDS. *Cancer Cell* **26**, 509–520 (2014).
55. Shuga, J., Zhang, J., Samson, L.D., Lodish, H.F. & Griffith, L.G. *In vitro* erythropoiesis from bone marrow-derived progenitors provides a physiological assay for toxic and mutagenic compounds. *Proc. Natl. Acad. Sci. USA* **104**, 8737–8742 (2007).
56. Gritsman, K. *et al.* Hematopoiesis and RAS-driven myeloid leukemia differentially require PI3K isoform p110- α . *J. Clin. Invest.* **124**, 1794–1809 (2014).
57. Mertins, P. *et al.* Integrated proteomic analysis of post-translational modifications by serial enrichment. *Nat. Methods* **10**, 634–637 (2013).
58. Rappsilber, J. & Mann, M. Analysis of the topology of protein complexes using cross-linking and mass spectrometry. *Cold Spring Harb. Protoc.* doi:10.1101/pdb.prot4594 (2007).
59. Beier, F. *et al.* Telomere-length analysis in monocytes and lymphocytes from patients with systemic lupus erythematosus using multicolor flow-FISH. *Lupus* **16**, 955–962 (2007).
60. Beier, F. *et al.* Accelerated telomere shortening in glycosylphosphatidylinositol (GPI)-negative compared with GPI-positive granulocytes from patients with paroxysmal nocturnal hemoglobinuria (PNH) detected by proaerolysin flow-FISH. *Blood* **106**, 531–533 (2005).